



BRNO UNIVERSITY OF TECHNOLOGY

VYSOKÉ UČENÍ TECHNICKÉ V BRNĚ

FACULTY OF MECHANICAL ENGINEERING

FAKULTA STROJNÍHO INŽENÝRSTVÍ

INSTITUTE OF PROCESS ENGINEERING

ÚSTAV PROCESNÍHO INŽENÝRSTVÍ

DESIGN OF MODULAR TUBULAR HEAT EXCHANGER

NÁVRH MODULOVÉHO TRUBKOVÉHO VÝMĚNÍKU TEPLA

MASTER'S THESIS

DIPLOMOVÁ PRÁCE

AUTHOR

AUTOR PRÁCE

Sven Marx

SUPERVISOR

VEDOUCÍ PRÁCE

doc. Ing. Zdeněk Jegla, Ph.D.

DOUBLE DEGREE COORDINATOR

DOUBLE DEGREE KOORDINÁTOR

Prof. Dr.-Ing. Marcus Reppich

BRNO 2020

Zadání diplomové práce

Ústav:	Ústav procesního inženýrství
Student:	Sven Marx
Studijní program:	Strojní inženýrství
Studijní obor:	Procesní inženýrství
Vedoucí práce:	doc. Ing. Zdeněk Jegla, Ph.D.
Akademický rok:	2019/20

Ředitel ústavu Vám v souladu se zákonem č.111/1998 o vysokých školách a se Studijním a zkušebním řádem VUT v Brně určuje následující téma diplomové práce:

Návrh modulového trubkového výměníku tepla

Stručná charakteristika problematiky úkolu:

Práce je zaměřena na rozměrový návrh modulového výměníku tepla s příčně obtékaným svazkem trubek pro využití odpadního tepla ze zanášivých spalin na zkušebně hořáků Ústavu procesního inženýrství. Účelem je s pomocí dostupné softwarové podpory navrhnout rozměry výměníku na základě tepelně–hydraulického výpočtu a dále provést výpočtovou analýzu rovnoměrnosti distribuce pracovní látky proudící uvnitř trubkového systému výměníku.

Cíle diplomové práce:

1. Seznámit se s problematikou návrhu trubkových výměníků modulového typu s křížovým tokem pracovních látek pro využití odpadního tepla spalin se zaměřením na aplikace pro zanášivé spaliny
2. S pomocí dostupného softwaru na základě tepelně–hydraulických výpočtů stanovit vhodné rozměry trubkového modulového výměníku tepla pro konkrétní využití odpadního tepla ze zanášivých spalin na zkušebně hořáků Ústavu procesního inženýrství.
3. S pomocí dostupného softwaru pro výpočtovou dynamiku proudění provést výpočtovou analýzu rovnoměrnosti distribuce pracovní látky proudící uvnitř trubkového systému modulového výměníku.
4. Provést souhrnné zhodnocení dosažených výsledků a zpracovat sestavný výkres navrženého výměníku.

Seznam doporučené literatury:

STEHLÍK P., Up-to-Date Waste-to-Energy Approach. From Idea to Industrial Application, SpringerBriefs in Applied Sciences and Technology, SpringerNature, Switzerland, 2016.

VDI-Gesellschaft Verfahrenstechnik und Chemieingenieurwesen Ed., VDI Heat Atlas, Second Edition, Springer-Verlag Berlin Heidelberg, 2010.

Termín odevzdání diplomové práce je stanoven časovým plánem akademického roku 2019/20

V Brně, dne

L. S.

prof. Ing. Petr Stehlík, CSc., dr. h. c.
ředitel ústavu

doc. Ing. Jaroslav Katolický, Ph.D.
děkan fakulty

Declaration

I hereby declare that I have authored this thesis independently, that I have not used other than the declared sources / resources, and that I have explicitly marked all material which has been quoted either literally or by content from the used sources. The master thesis was solely written and used in terms of the Double Degree Program between University of Applied Science Augsburg (HAS) and Brno University of Technology (BUT).

Abstract

The main goal of this thesis is to get acquainted with the process requirements and the design of a cross flow heat exchanger, as well as evaluating the design with the help of simulation software. First the operation conditions for waste heat recovery and general design options are examined and the basic thermal and hydraulic equations are presented. The main part of this thesis concentrates on a modular cross flow tubular heat exchanger proposed for experimental research of the heat recovery and fouling process of the flue gas produced from the combustion of alternative at Brno University of Technology (BUT) at the Institute of Process Engineering (UPI). First the given situation in the testing laboratory is briefly explained. Then the simulation of the proposed heat exchanger design with the software HTRI is described and the results are summarized and compared with the target requirements for the design. The tube-side water flow distribution inside of one of four identical heat exchanger modules is analyzed with the help of CFD software using three different simulation approaches. Two approaches using the $k-\omega$ -SST turbulence model and one using the $k-\epsilon$ -Realizable turbulence model are described from generating the CAD model over meshing and setting the boundary condition to running the simulation. In the end the differences between the approaches and results of the flow distribution simulations are discussed.

Keywords

Crossflow Heat Exchanger, Heat Recovery, HTRI, CFD, Flow Distribution, k - ω -SST, k - ϵ -Realizable

Table of Contents

Objective of Work	1
Declaration	3
Abstract	4
Keywords.....	4
Table of Contents	5
Table of Figures.....	6
Table of Tables	8
List of Symbols and Abbreviations	9
1 Introduction.....	10
1.1. Flue gas waste heat utilization in process industry.....	10
1.2. Heat exchangers for flue gas waste heat utilization	11
1.2 Basic equation for thermal-hydraulic design of heat exchangers.....	13
1.2.1 Heat and Mass Flow balance of Heat exchangers	13
1.2.2 Flow parameters and heat transfer for planar wall	15
1.2.3 Heat transfer and flow through pipes	16
1.2.4 Stream properties for forced convection	20
2. Design of modular heat exchanger	23
2.1 Introduction to design of modular heat exchanger – description of situation, input data and design constraints	23
2.2 Thermal-hydraulic design of modular heat exchanger using HTRI Xchanger Suite 25	25
2.3 Main design results.....	29
3 Analysis of uniformity of water distribution inside one tubular module of heat exchanger.....	31
3.1 Creation of a model for CFD simulation	31
3.1.1 Geometry.....	32
3.1.2 Mesh and numerical model	32
3.2 Setting of simulation conditions and run of simulation	44
3.3 Main results of CFD simulation	47
4 Conclusion.....	53
References	55
Appendix.....	56

Table of Figures

Figure 1: Coal combustion plant with boiler and economizer [1, p. 1304].....	11
Figure 2: Actual pattern of ash deposition on H-type finned tube heat exchanger at different gas velocities after 18 hours at flue gas velocities (a) 4.5 m·s ⁻¹ ; (b) 6.25 m·s ⁻¹ , for gas with high ash content. [2, p. 4683].....	12
Figure 3: Flue gas heat exchanger [3].....	12
Figure 4: Combustion air preheaters [3].....	12
Figure 5: Flue Gas Heat Exchanger [4].....	12
Figure 6: Flue Gas Heat Exchanger Welded Pillows [4].....	12
Figure 7: Flue Gas Heat Exchanger (Tubular, Crossflow) [4].....	13
Figure 8: Schematic diagram of a heat exchanger [5, p. 34].....	14
Figure 9: Temperature profile in a semi-infinite body [5, p. 23].....	18
Figure 10: Contact temperature T_m between two semi-infinite bodies. [5, p. 23].....	19
Figure 11: Cooling of a plane plate [5, p. 24].....	19
Figure 12: Tube bundle measurements [5, p. 26].....	22
Figure 13: Current situation at the research furnace.....	23
Figure 14: Future situation at the research furnace.....	24
Figure 15: Sketch future modular heat exchanger.....	25
Figure 16: Water distribution and collection for one module.....	25
Figure 17: Serpentine of one heat exchanger tube.....	25
Figure 18: HTRI Xchanger Suite: Input summary.....	26
Figure 19: HTRI Xchanger Suite: tube geometry.....	27
Figure 20: HTRI Xchanger Suite: bundle geometry.....	27
Figure 21: HTRI Xchanger Suite: tubes of one tube bundle / module.....	28
Figure 22: Top View of Heat Exchanger Module.....	31
Figure 23: Global settings and properties of small k- ω mesh.....	33
Figure 24: Histogram elements - y^+ with curve of cumulative percentage.....	34
Figure 25: Meshed geometry with colored regions.....	35
Figure 26: 0,02 mm x 5 Inflation at distributor (a) and collector (b) with detail view of the transition from inflation layers to the core mesh of the distributor (c).....	35
Figure 27: 0,014 mm x 5 Inflation at serpentine (a) with detail view of the transition from inflation layers to the core mesh(b).....	35
Figure 28: Skewed cells of the small k- ω mesh (skewness > 0,5).....	36
Figure 29: Contour plot - y^+ values of the small k- ω model (Scale [0; 6,19]).....	37
Figure 30: 0,0083 mm x 24 Inflation at collector.....	39
Figure 31: 0,007 mm x 24 Inflation at serpentine.....	39
Figure 32: Skewed cells of the big k- ω mesh (skewness > 0,5).....	39
Figure 33: 2,4 mm x 1 Inflation at distributor.....	41
Figure 34: 2,4 mm x 1 Inflation at serpentine.....	41
Figure 35: Skewed cells of the k- ϵ mesh (skewness > 0,5).....	42
Figure 36: y^+ -histogram of k- ϵ mesh with curve of accumulated percentages.....	43
Figure 37: Contour plot - y^+ values of the k- ϵ model.....	43
Figure 38: Control Surfaces (YZ-Plane trough the distributor, XZ-Plane trough the first serpentine and Monitors as well as Surfaces at the tube Inlets for reference pressures) and Points (one in the turbulent part of the distributor and one in the turbulent part of the first serpentine) for the evaluation of simulation results and convergence.....	46
Figure 39: Residuals k- ω small – steady state.....	46
Figure 40: Residuals k- ϵ - steady state – transient 0,2s timesteps.....	47
Figure 41: contour plot of velocity in YZ-plane of the distributor and serpentines (k- ω small); (scale [0; 1,32] m/s).....	48

Figure 42: contour plot of velocity in YZ-plane of the distributor and serpentines (k- ω big); (scale [0; 1,31] m/s).....	48
Figure 43: contour plot of velocity in YZ-plane of the distributor and serpentines (k- ϵ); (scale [0; 1,3] m/s)	48
Figure 44: Vector plot of middle plane of the two upper Serpentine inlets (k- ω big) (scale [0; 1,32] m/s)	48
Figure 45: Plot of Mass Flow Rates over Time for big k- ω mesh - Time Steps of 0,005 s	49
Figure 46: Plot of Mass Flow Rates over Time for k- ϵ mesh - Time Steps of 0,20 s	49
Figure 47: Mass flow distribution.....	50
Figure 48: Contour Plot of Static pressure in the YZ-plane of the distributor with first straight parts of the tubes (k- ϵ simulation).....	52
Figure 49: Contour Plot of Static Pressure in the XZ-Plane of the first serpentine (k- ϵ simulation)	52

Table of Tables

Table 1: HTRI Input A	28
Table 2: HTRI input B	28
Table 3: HTRI input C	29
Table 4: Results HTRI simulation - Air / Gas	29
Table 5: Results HTRI simulation - water	30
Table 6: Tube dimensions - final design.....	31
Table 7: Used methods and settings for k- ω mesh	34
Table 8: Element metrics of small k- ω mesh.....	36
Table 9: Mesh set up big k- ω mesh	38
Table 10: Mesh Metrics - big k- ω mesh	39
Table 11: Mesh set up k- ϵ mesh	41
Table 12:Element metrics of k- ϵ mesh	42
Table 13: Simulation settings (1/2).....	44
Table 14: Setting of the Solution Methods (2/2)	45
Table 15: Mass Flow Rates and Standard Deviations for each case.....	50
Table 16:Deviation of Target Mass Flow Rates for each tube and for each case in percent.....	50
Table 17: Inlet and outlet pressures in Tubes and Total Pressure drop of Heat Exchanger Module In- to Outlet.....	51

List of Symbols and Abbreviations

Symbol	Unit	Quantity
A	m^2	Area
b	$W \cdot s^{1/2} / m^2 \cdot K$	Heat Penetration Coefficient
Bi	-	Biot Number
c_p	$J/kg \cdot K$	Specific Heat Capacity at constant pressure
d_h	m	Hydraulic Diameter
E	J	Energy
h	J/kg	Mass Specific Enthalpy
k	$W/m^2 \cdot K$	Overall Heat Transfer Coefficient
L	m	Length
Nu	-	Nusselt Number
\dot{M}	kg/s	Mass Flow Rate
p	Pa	Pressure
Pr	-	Prandtl Number
Q	J	Heat
\dot{q}	W	Heat Flux
R	$J/kg \cdot K$	Individual Gas Constant
r	m	Radius
Re	-	Reynolds Number
t	S	Time
T	K	Absolute Temperature
W	J	Work
w	m/s	Average Velocity
\dot{W}	$J/kg \cdot K \cdot s$	Heat Capacity Rate
x	m	Length in Direction of Heat Conduction
z		Coordinate perpendicular to flow direction
α	$W/m^2 \cdot K$	Heat Transfer Coefficient
δ	m	Thickness
η	$Pa \cdot s$	Dynamic Viscosity
Θ	K	Temperature difference
λ	$W/m \cdot K$	Thermal Conductivity
ν	m^2/s	Kinematic Viscosity
ξ	-	Friction Factor
ρ	kg/m^3	Density

1 Introduction

At Brno University of Technology (VUT Br) at the Institute of Process Engineering (UPI) of the Faculty of Mechanical Engineering (FSI), research on industrial applications is done. There is a lot of emphasis on thermal processes and therefore, heat exchange is an important part of the research. This thesis' aims are to give a brief information over the basic considerations concerning heat exchangers for the utilization of flue gas waste heat and related basic calculations. Furthermore, a newly constructed modular crossflow heat exchanger is to rate, its streams are to be simulated and evaluated regarding their flow distribution.

1.1. Flue gas waste heat utilization in process industry

In a lot of processes, the efficiency is strongly limited by the amount unused heat. The heat, that is not used in the primary process is referred to as waste heat. Depending on the process waste heat can be defined differently. In case of a turbine or a motor, this would be the energy of the hot flue gas. As an incinerator's primary task is to minimize the amount of waste that needs to be deposited and its toxicity, all the heat released in this process could be defined as waste heat. Often the use of waste heat is described with the term heat recovery. For heat recovery there are different options. Most common are recuperators, which transfer heat between fluids. A second option are regenerators, in which heat from a fluid is transferred to a solid material and thereafter from the solid material to another fluid. And lastly, there are thermoelectric elements, that change thermal energy into electric energy directly. This however is neither very efficient and nor commonly used industrially. Therefore, this will not be mentioned any further.

With an increasing amount of waste heat, using it for further processes or heating is a way to increase the overall efficiency of the process complex by far, as less heat is released into the environment, without use. The simplest way of using the waste heat of thermal processes might be preheating of the fluids, entering the process using the hot product streams. The apparatus used therefore is mostly referred to as an economizer. If the amount of waste heat and the temperature are high, more complex approaches of using the waste heat can be realized.

Combustion plants primarily use the generated heat to drive a Rankine Cycle, a gas turbine, or a big engine. The waste heat is used for preheating the combustion air, drying the coal or even to treat the flue gas (denitrification) [1]. Some heat might also be used in nearby industry or to heat households if a heat distribution net is given.

For an incinerator, literally any use of the produced heat is to be considered using the waste heat. As the heat released by the combustion of the waste in the burning chamber reaches high values and needs to be transferred out of the burning chamber anyways, it only makes sense to use it analogue a coal combustion plant. The heat is transferred into water pipes in the walls of the combustion chamber and heat exchangers along the path of the flue gas, to cool down the walls, boil the water and superheat the steam. This usually is part of a Rankine Cycle in order to first convert heat into mechanical and then into electric energy. The waste heat of the Rankine Cycle can be utilized for heating of households by means of a heat distribution network. The rest heat of the flue gas again can be used for the flue gas treatment to decrease its toxicity (i.e. SNCR; SCR).

Industrial parks use the waste heat of strongly exothermal processes to heat processes that need additional heat. This is generally done by using superheated steam as carrier medium for the heat, which can easily and safely be transported in insulated pipes and has a relative high energy density.

1.2. Heat exchangers for flue gas waste heat utilization

The choice of the heat exchanger is strongly depending on the composition of the flue gas. If a clean fuel like natural gas is burned, the flue gas will mostly consist of humid air and carbon dioxide [2, p. 97]. In this case, fouling on the gas side will not be of great importance and basically any heat exchanger, that can cope with the temperature and pressure given, is suited. Shell and tube heat exchangers in counter current flow arrangement would be fitting. They can be used for temperatures up to 1100 °C, from high vacuum up to 100 MPa and have a high heat transfer to volume ratio [1]. Furthermore, they are available in a huge range of sizes. A crossflow heat exchanger might be fitting as well. The less efficient crossflow arrangement can be compensated by fins on the tubes. If the fins, follow the direction of the flow, a highly increased pressure drop can be avoided. As the fins can be in perfect alignment with the flow direction, the low-pressure drop might be considered an advantage over a shell and tube application, especially where the pressure drop is to be kept as low as possible (e.g. turbine outlet). Regenerators are another option if indirect contact of the hot and cold stream is acceptable.

However, the flue gas of most large-scale incinerators, furnaces (Figure 1) or in general combustion plants will have ash content. Due to this, the contact surface of the heat exchangers and the flue gas should be designed in a way that they are easy to clean and prevent particles to stick to or lay on them. This leads to two restrictions. Firstly, the heat exchanger cannot be permanently closed as it would make the inside inaccessible for frequent cleaning or fouling removal. Secondly, fins might be inconvenient, as they create hard to clean surfaces and corners for fouling layers to stick to, or ash to accumulate. This can lead to serious problems due to excessive fouling within short time, as to see in (Figure 1). Due to this heat exchangers for ash containing flue gas, in most cases, consist of tube bundles hanging freely in the flue gas stream. The fouling layer can be brushed or blown off and falls down, where the ash is collected, during the cleaning process (Figure 3).

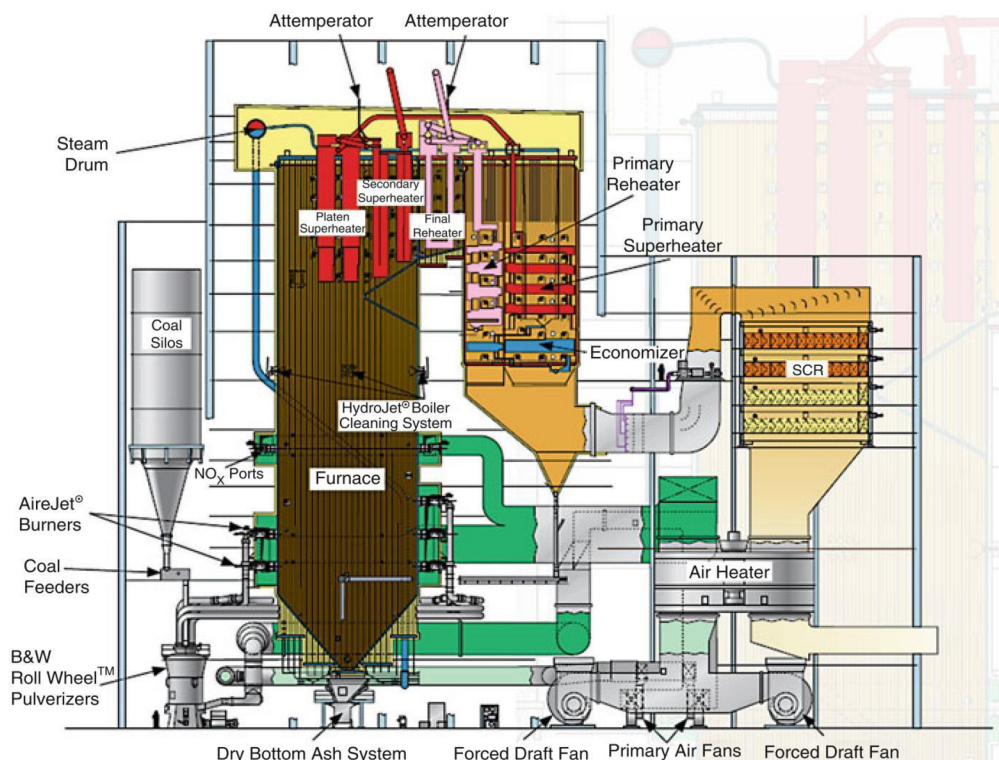


Figure 1: Coal combustion plant with boiler and economizer [1, p. 1304]



Figure 2: Actual pattern of ash deposition on H-type finned tube heat exchanger at different gas velocities after 18 hours at flue gas velocities (a) 4.5 m·s-1; (b) 6.25 m·s-1, for gas with high ash content. [2, p. 4683]



Figure 3: Flue gas heat exchanger [3]

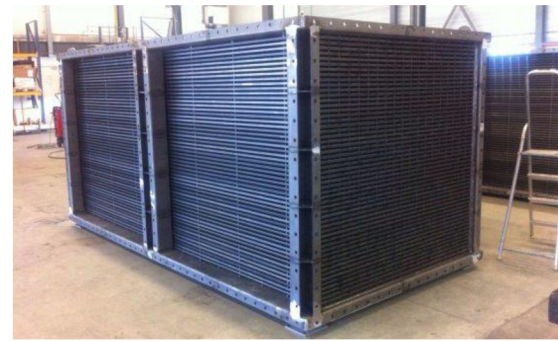


Figure 4: Combustion air preheaters [3]

Combustion air preheaters (Figure 4) mostly are applied after the cleaning process of the flue gas and therefore can be build compacter. For some applications even 3D-structures are used to save space or heat catalytic structures.

For flue gas without particles even welded plate heat exchangers or hybrids like crossflow heat exchangers with welded pillows can be used for heat recovery. (Figure 5, Figure 6)



Figure 5: Flue Gas Heat Exchanger [4]



Figure 6: Flue Gas Heat Exchanger Welded Pillows [4]



Figure 7: Flue Gas Heat Exchanger (Tubular, Crossflow) [4]

The right type of heat exchanger depends on the given process conditions and must be chosen accordingly. If particles and strong fouling are involved, cleaning must be considered. Tubes without fins might be the best solution for process conditions, prone to fouling. Finning (Figure 7) might be convenient in cases where the gas is clean. This especially applies if the cooling fluid is liquid, so the heat transfer area on the gas side is enhanced for a more efficient heat transfer. This is because the film heat transfer coefficient for gases in general is a lot lower, than for liquids. In the end the heat duty and the pressure drop on both sides must be congruent with the process requirements, even with a buildup fouling layer. So, there is a lot to consider for choosing the right heat exchanger and it would be a huge advantage to know more about the fouling that is to be expect in advance.

1.2 Basic equation for thermal-hydraulic design of heat exchangers

The following basic equations and explanations are all based on the VDI Heat Atlas [5]. It is always assumed, that a steady state is given, and the calculations are performed with averaged values. This is valid for heat exchangers that work under constant conditions.

The term heat is defined by the first law of thermodynamics as the energy that is transported across the boundary of a thermodynamic system due to a temperature difference between the system and its surroundings. The first law of thermodynamics in a general form can be written as follows: [5, p. 17]

$$\Delta E = W + Q + E_M \quad (1)$$

In words: The change of energy in a system equals the work (W), the heat (Q) and the Energy (E_M that is tied to a mass transport), that are transferred across the boundary of the system.

1.2.1 Heat and Mass Flow balance of Heat exchangers

The local heat flux (\dot{q}) at the heat transfer surface can be expressed with the local overall heat transfer coefficient (k_{loc}) and the local temperature difference. (2)

$$\dot{q} = k_{loc} \cdot (\theta_1 - \theta_2) \quad (2)$$

By integrating the local heat flux over the entire area of the heat transfer area the total heat flux (\dot{Q}) is calculated. (3)

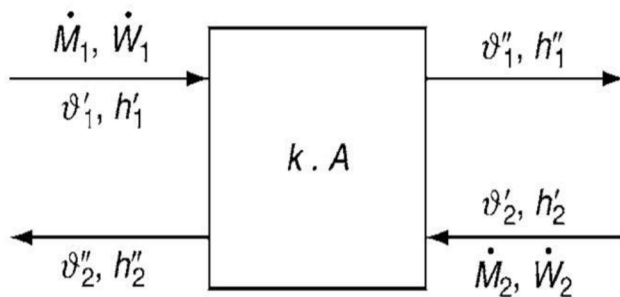
$$\dot{Q} = \int \dot{q} dA \quad (3)$$

By introducing the overall heat transfer coefficient (k) and the mean temperature difference ($\Delta\vartheta_m$) Equation (3) can be simplified and written like Equation (4).

$$\dot{Q} = kA\Delta\vartheta_m \quad (4)$$

“Using the energy balance equations for the two fluids in the heat exchanger, the heat flow rate transferred in steady state operation can be expressed in terms of the changes in enthalpy within the two streams.” (5) [5]

$$\dot{Q} = \dot{M}_1(h'_1 - h''_1) = \dot{M}_2(h'_2 - h''_2) \quad (5)$$



$\dot{M}_1, \dot{M}_2 =$ mass flow rates

$\dot{W}_1, \dot{W}_2 =$ heat capacity rates

$h_1, h_2 =$ specific enthalpies

$\vartheta_1, \vartheta_2 =$ temperatures

Figure 8: Schematic diagram of a heat exchanger [5, p. 34]

In Equation (5), energy exchange with the surrounding, kinetic and potential

Energies are ignored. The change in enthalpy can, in single-phase systems, be expressed as a change in temperature by introducing the heat capacity rate (\dot{W}). (6)

$$\dot{W}_i = \frac{\dot{M}_i(h'_i - h''_i)}{\vartheta'_i - \vartheta''_i} = \dot{M}_i c_{pm,i} \quad (6)$$

“If the enthalpy is independent of pressure (e.g., as in an ideal gas) or if the pressure drop in flow direction can be neglected (isobaric change of state), $c_{pm,i}$ is the mean specific heat capacity at constant pressure between the inlet and the outlet temperatures. If a phase change occurs in a system that consists of only one pure substance (and the pressure remains constant), the heat capacity flow rate becomes infinite. Equations (4),(5), and (6) can then be combined to Equation (7).” [5]

$$\dot{Q} = kA\Delta\theta_m = \dot{W}_1(\theta'_1 - \theta''_1) = \dot{W}_2(\theta'_2 - \theta''_2) \quad (7)$$

1.2.2 Flow parameters and heat transfer for planar wall

The resulting heat flow rate (\dot{Q}) and the heat flux (\dot{q}) are defined by Equations (8) and (9).

$$\dot{Q} = \frac{dQ}{dt} \quad (8)$$

$$\dot{q} = \frac{d\dot{Q}}{dA} \quad (9)$$

$$\dot{q} = -\lambda \frac{\partial T}{\partial x} \quad (10)$$

$$\dot{q} = \alpha(T_W - T_F) \quad (11)$$

The heat flux through a wall as a result of thermal conductivity (λ) is described in Equation (10). The heat transfer between wall (W) and fluid (F) results out of their temperature (T) difference and the heat transfer coefficient (α) (11). For calculation of the flow parameters of the fluid the Nusselt-, Reynolds- and Prandtl- Numbers are defined according to Equations (12),(13), (14). The parameters used for the calculation are the length (L), the average flow velocity (w), the kinematic viscosity (ν), the hydraulic diameter (d_h), the dynamic viscosity (η), the density (ρ) and the isobar specific heat capacity (c_p).

$$Nu = \frac{\alpha \cdot L}{\lambda} \quad (12)$$

$$Re = \frac{w \cdot L}{\nu} = \frac{w \cdot d_h \cdot \rho}{\eta} \quad (13)$$

$$Pr = \frac{\nu}{\frac{\lambda}{\rho \cdot c_p}} \quad (14)$$

Defining the temperature difference as in Equation (15) we can write the heat flow through a wall of an area (A) and a thickness (δ) as in Equation (16).

$$\Delta T = T_1 - T_2 \quad (15)$$

$$\dot{Q} = \frac{\lambda A}{\delta} \cdot \Delta T \quad (16)$$

Analogue to electric resistance, thermal resistance (R) is defined as in (17) and defined for conductive heat transfer (18).

$$R = \frac{\Delta T}{\dot{Q}} \quad (17)$$

$$R_{cond} = \frac{\delta}{\lambda A} \quad (18)$$

1.2.3 Heat transfer and flow through pipes

The heat flow rate through a cylindrical area, according to Fourier's law, can be written as in (19). The radius (r) and the circle number (π) are needed here.

$$\dot{Q} = -\lambda 2\pi r L \frac{dT}{dr} \quad (19)$$

That leads to Equation (20) in order to calculate the temperature (T_i) on a radius (r_i) within a cylindrical body. Out of this the heat flow through a pipe (21) can be derived, where the outer radius (r_o) and outer temperature (T_o) are given.

$$T_i - T = \frac{\dot{Q}}{\lambda 2\pi L} \ln \frac{r}{r_i} \quad (20)$$

$$\dot{Q} = -\lambda 2\pi r L \frac{T_i - T_o}{\ln \frac{r_o}{r_i}} \quad (21)$$

By defining the average heat transfer area A_m (22) with the inner and outer surfaces of a pipe A_i (23) and A_o (24), the heat flow can be written analogue to the heat conduction through a planar wall as in Equation (25).

$$A_m = \frac{A_o - A_i}{\ln \frac{A_o}{A_i}} \quad (22)$$

$$A_o = 2\pi r_o L \quad (23)$$

$$A_i = 2\pi r_i L \quad (24)$$

$$\dot{Q} = \lambda A_m \frac{T_i - T_o}{\delta} \quad (25)$$

For a pipe, then the thermal resistance of conduction is defined as in (26).

$$R_{cond} = \frac{\ln \frac{r_o}{r_i}}{\lambda 2\pi L} \quad (26)$$

The convective thermal resistance is defined as the inversion of the heat transfer coefficient divided by the heat transfer area (27).

$$R_{conv} = \frac{1}{\alpha A} \quad (27)$$

For a planar wall, the overall heat transfer coefficient is the sum of the convective thermal resistances of both sides of the wall and the sum of conductive thermal heat transfer resistances of all layers of the wall. (28)

$$R = \frac{1}{kA} = \frac{1}{\alpha_i A} + \sum_j \frac{\delta_j}{\lambda_j A} + \frac{1}{\alpha_o A} \quad (28)$$

Using the analogy of the conduction through a tube wall and a planar wall, given by using the average heat transfer area, we can calculate the overall heat transfer resistance of a pipe with Equation (29). Here the index *i* stands for inner, *o* for outer and *j* for a count of a wall layer. A_j is to be calculated for each layer of the wall according to Equation (30).

$$R = \frac{1}{kA} = \frac{1}{\alpha_i A_i} + \sum_j \frac{\delta_j}{\lambda_j A_{mj}} + \frac{1}{\alpha_o A_o} \quad (29)$$

Usually the fouling layer is not calculated as an extra layer on the wall, but a fouling resistance R_f is added on both sides for both sides of the wall. The values are chosen from tables with values for different fluids and flow velocities.

$$A_{mj} = \frac{A_{oj} - A_{ij}}{\ln \frac{A_{oj}}{A_{ij}}} \quad (30)$$

As the temperature of a certain location in a heat exchanger which operates steadily remains the same over time, the model of a semi-infinite body is applied, as the streaming fluid keeps the core temperature constant. The temperature (T) of a point in a semi-infinite body is calculated using the initial temperature of the body (T_0) and the environmental temperature (T_{env}) to which the surface is cooled down and which stays constant. The difference between the temperature on the searched spot and the environmental temperature divided by the difference of the initial body temperature and the temperature of the environment equals the Gaussian Error Function. (31)

$$\frac{T - T_{env}}{T_0 - T_{env}} = f\left(\frac{x}{\sqrt{at}}\right) \quad (31)$$

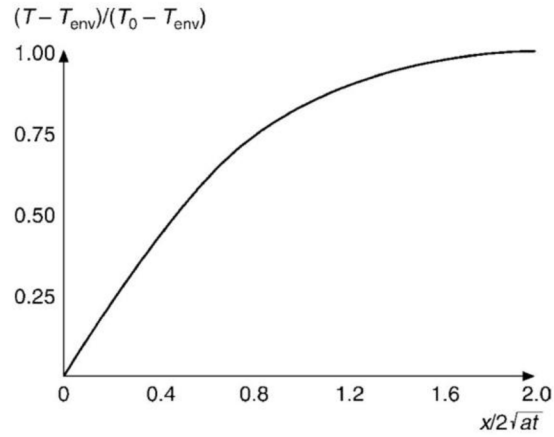


Figure 9: Temperature profile in a semi-infinite body [5, p. 23]

$$\dot{q} = \frac{b}{\sqrt{\pi t}} (T_{env} - T_0) \quad (32)$$

$$b = \sqrt{\lambda \rho c} \quad (33)$$

By differentiation of the heat flow at the surface one gets Equation (32) with the heat penetration coefficient (b) (33).

As in a heat exchanger both sides of a wall will be heated or cooled by a constant stream of fluid, a model of two semi-infinite bodies in contact is a quite accurate approximation. The heat flux is then written like in Equation (34).

$$\dot{q} = \frac{b}{\pi t} (T_{env} - T_0) \Phi(z) \quad (34)$$

$$\Phi(z) = 1 - \frac{1}{2z^2} + \frac{1 \cdot 3}{2^2 z^4} - \dots + (-1)^{n-1} \frac{1 \cdot 3 \dots (2n-3)}{2^{n-1} z^{2n-2}} \quad (35)$$

$$z = \alpha \frac{\sqrt{at}}{\lambda} \quad (36)$$

The contact temperature between the two semi-infinite bodies (Figure 9) is calculated using Equation (37).

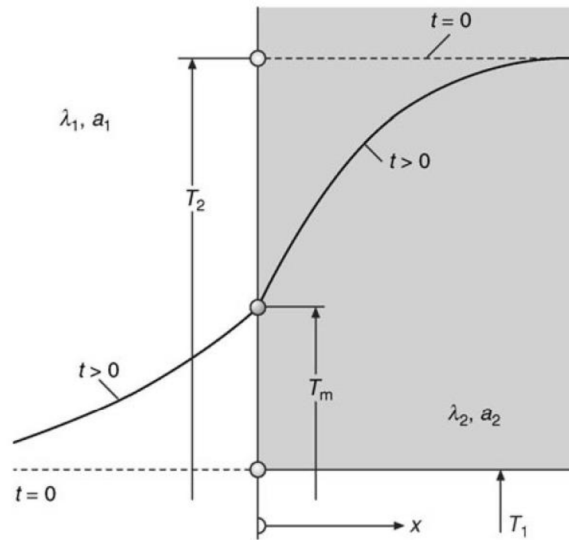


Figure 10: Contact temperature T_m between two semi-infinite bodies. [5, p. 23]

$$\frac{T_m - T_1}{T_2 - T_1} = \frac{b_2}{b_1 + b_2} \quad (37)$$

For a plane plate and a ratio of $\frac{at}{X^2} \geq 0,24$ Equation (38) provides a good approximation for the heat profile (Figure 11).

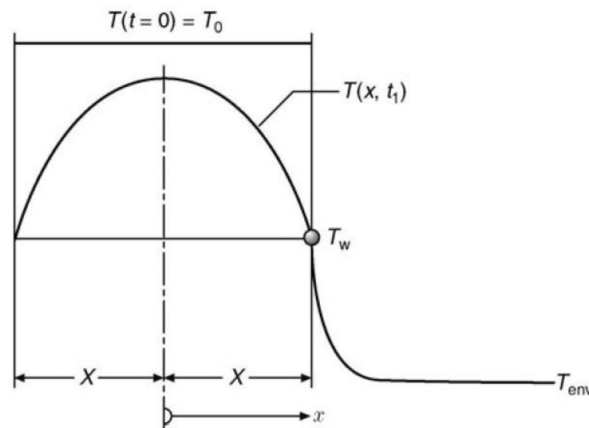


Figure 11: Cooling of a plane plate [5, p. 24]

$$\frac{T - T_{env}}{T_0 - T_{env}} = C \exp\left(-\delta^2 \frac{at}{X^2}\right) \cos\left(\delta \frac{x}{X}\right) \quad (38)$$

The constants C and δ depend on the Biot Number (39) according to Table B1. Table 1 in the VDI Heat Atlas 2010.

$$Bi = \frac{aX}{\lambda} \quad (39)$$

For a cylinder x is replaced with the radius (r) and X with the radius of the cylinder (R). For this approximation, the ratio of $\frac{at}{R^2} \geq 0,21$ must be given to be considered valid. The constants C and δ are to be found in B1. Table 2 of the VDI Heat Atlas 2010, after calculating the Biot Number.

$$\frac{T - T_{env}}{T_0 - T_{env}} = C \exp\left(-\delta^2 \frac{at}{R^2}\right) I_0\left(\delta \frac{x}{R}\right) \quad (40)$$

1.2.4 Stream properties for forced convection

For a laminar flow along a flat plate of a Length (L) the Nusselt Number is calculated with Equation (41), where Re and Pr are calculated according to the Equations (13) and (14). A flow is considered laminar if the Reynold Number doesn't exceed 2300.

$$Nu = 0.664 Re^{\frac{1}{2}} Pr^{\frac{1}{3}} \quad (41)$$

For turbulent flow along a plate Equation (42) holds.

$$Nu = \frac{0.037 Re^{0.8} Pr}{1 + 2.443 Re^{-0.1} \left(Pr^{\frac{2}{3}} - 1 \right)} \quad (42)$$

The mean heat transfer coefficient α depends on the heat flux (43) and the logarithmic mean temperature difference (ΔT_m) with wall temperature (T_w) and the inner and outer temperatures (T_{in} and T_{out}).

$$\dot{q} = \alpha \Delta T_m \quad (43)$$

$$\Delta T_m = \frac{(T_w - T_{in}) - (T_w - T_{out})}{\ln \frac{T_w - T_{in}}{T_w - T_{out}}} \quad (44)$$

For laminar flow through pipes Equation (45) is to be used to find the Nusselt Number.

$$Nu_0 = \frac{3.657}{\tan h\left(2.264 X^{\frac{1}{3}} + 1.7 X^{\frac{2}{3}}\right)} + \frac{0.0499}{X} \tan h X \quad (45)$$

If a fluid enters a pipe at an approximately constant velocity, the velocity profile changes along the flow path until it reaches the Poiseuillean Parabola after a distance L_{entry} described by the equation $L_{entry} / (d Re) = 5,75 * 10^2$. For a hydrodynamically developed laminar flow, Equation ((46) holds for the range $0,1 \leq Pr \leq \infty$.

$$\frac{Nu}{Nu_0} = \frac{1}{\tan h\left(2.34 Pr^{\frac{1}{6}} X^6\right)} \quad (46)$$

In case of a hydrodynamically developed turbulent flow for $L / d \geq 60$ and a ranges of $Re \in [10^4; 10^5]$ and $Pr \in [0,5; 100]$ Equation (47) holds.

$$Nu = 0.024 Re^{0.8} Pr^{\frac{1}{3}} \quad (47)$$

If $Re \in [10^5; 10^6]$ and $Pr \in [0,6; 1000]$ Equation (48) is to use.

$$Nu = \frac{Re Pr \frac{\zeta}{8}}{1 + 12.7 \sqrt{\frac{\zeta}{8}} (Pr^{\frac{2}{3}} - 1)} \left[1 + \left(\frac{d}{L} \right)^{\frac{2}{3}} \right] \quad (48)$$

For a bend in a pipe with a diameter (D) the Equation (49) holds for turbulent flow.

$$\alpha = \alpha_{straight} \left[1 + (21Re^{0.14}) \left(\frac{d}{D} \right) \right] \quad (49)$$

For a pipe placed transversal in a flow (e.g. crossflow) the Nusselt Number can be calculated out of the Nusselt Number for laminar plate flow (41) and turbulent plate flow (42).

$$Nu = 0.3 + (Nu_{lam}^2 + Nu_{turb}^2)^{\frac{1}{2}} \quad (50)$$

$$L = \frac{d\pi}{2} \quad (51)$$

The flow in between pipe bundles is described as follows in (52) - (58). The measurements are visualized in Figure 12.

$$Re = \frac{w_m L}{\nu} \quad (52)$$

$$w_m = w\Psi \quad (53)$$

$$a = \frac{s_1}{d} \quad (54)$$

$$b = \frac{s_2}{d} \quad (55)$$

$$\Psi = 1 + -\frac{\pi}{4ba} \quad (56)$$

$$Nu_B = f_A Nu \quad (57)$$

$$f_A = 1 + 0.7 \frac{\frac{b}{a} - 0.3}{\Psi^{\frac{3}{2}} \left(\frac{b}{a} + 0.7 \right)^2} \quad (58)$$

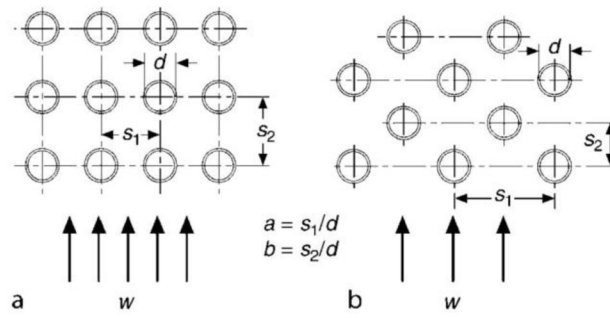


Figure 12: Tube bundle measurements [5, p. 26]

Finally, the pressure drop can be calculated with the Darcy Weißbach Equation (59).

$$\Delta p = \frac{w^2}{2} \cdot \rho \cdot \left(\frac{L}{d_h} \cdot \lambda + \sum \zeta \right) \quad (59)$$

2. Design of modular heat exchanger

The design of a heat exchanger is a sophisticated process which acquires knowledge and experience. First a primary design must be chosen, fitting for the needs of the process. Therefore, in addition to the heat duty, allowable pressure drops, chemical and pressure resistance, accessibility for cleaning and maintenance has to be considered. Once the primary design is developed, the sizing of the components must be done in order to achieve the wanted heat duty. This process consists of iterative circles of rating the current design and adjusting parameters, until the final design is reached. Nowadays, computer programs such as *HTRI Xchanger Suite* allow for a fast, iterative process.

2.1 Introduction to design of modular heat exchanger – description of situation, input data and design constraints

At the Faculty of Mechanical Engineering (FSI) at the burners testing laboratory of the Institute for Process Engineering (UPI) a rotating furnace (Figure 13) for research on combustion processes is given (Figure 13). At the moment the exhaust flue gas, with a temperature of about 950°C, is simply lead off through a DN200 steel pipe.

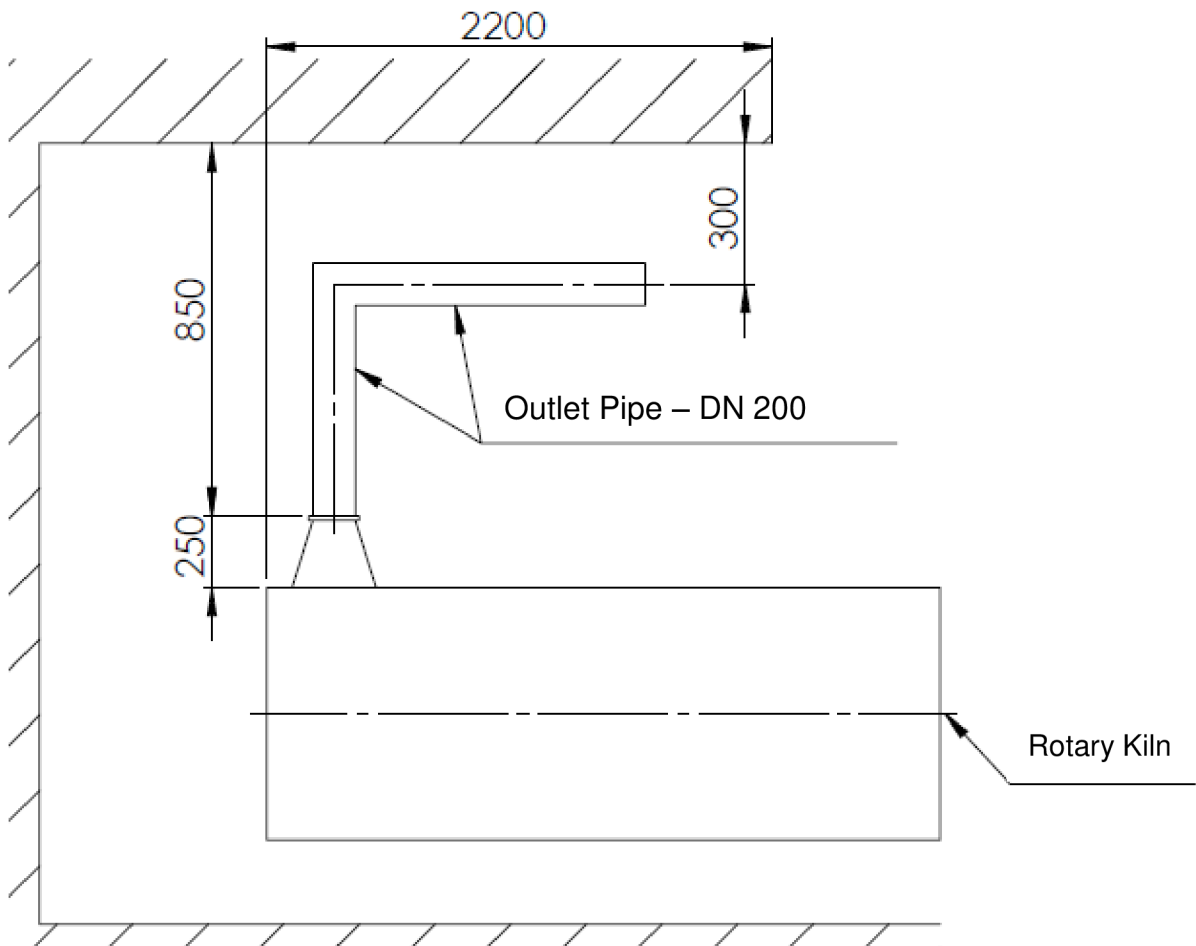


Figure 13: Current situation at the research furnace

As research on heat exchangers is also performed at UPI, the chance to use the furnace to study fouling processes in heat exchangers was recognized. The exhaust gas could be cooled down with a heat exchanger, to mimic industrial conditions of a heat regenerator. For this purpose, a heat exchanger with easy access to the pipes is necessary, as the buildup fouling layer on them is to be examined to gain knowledge about the fouling process. The heat exchanger material needs to be fitting for any fuels burned in the furnace and should cool down the exhaust gas to 450 – 460 °C. The pressure drop on the gas side should not exceed 100 Pa, while the pressure drop for the cooling water on the tube side should be lower than 1 kPa. At the same time, the cooling water temperature of 20 °C should not increase to more than 30 °C. As often for flue gas waste heat recovery a crossflow heat exchanger shall be used. It makes sense to use a crossflow design, to gain directly applicable knowledge. For easy access to the tubes the heat exchanger is built modular, so that the tube bundles can be removed for investigation. To manage the required heat duty, four modules of six horizontally parallel serpentine with four tube passes each are found to be required. The serpentine are operated in counter current to the flue gas (Figure 14, Figure 15). The cooling water of the six pipes per module is distributed and collected with a distributor or collector tube. The serpentine tubes consist of carbon steel and measure 26,9 x 2,3 mm with a bed radius of 29 mm (Figure 17). The straight part of the serpentine is 400 mm long. The distributor pipe has an inner diameter of 57 mm and the collector pipe measures 76,1 mm on the inside (Figure 16). The design is to be rated with HTRI Xchanger Suite. As the furnace is operated with different fuels, as flue gas air was chosen for the HTRI simulation. This is because for air sufficient data for simulation is given and assumptions on flue gas would only be valid for a specific fuel.

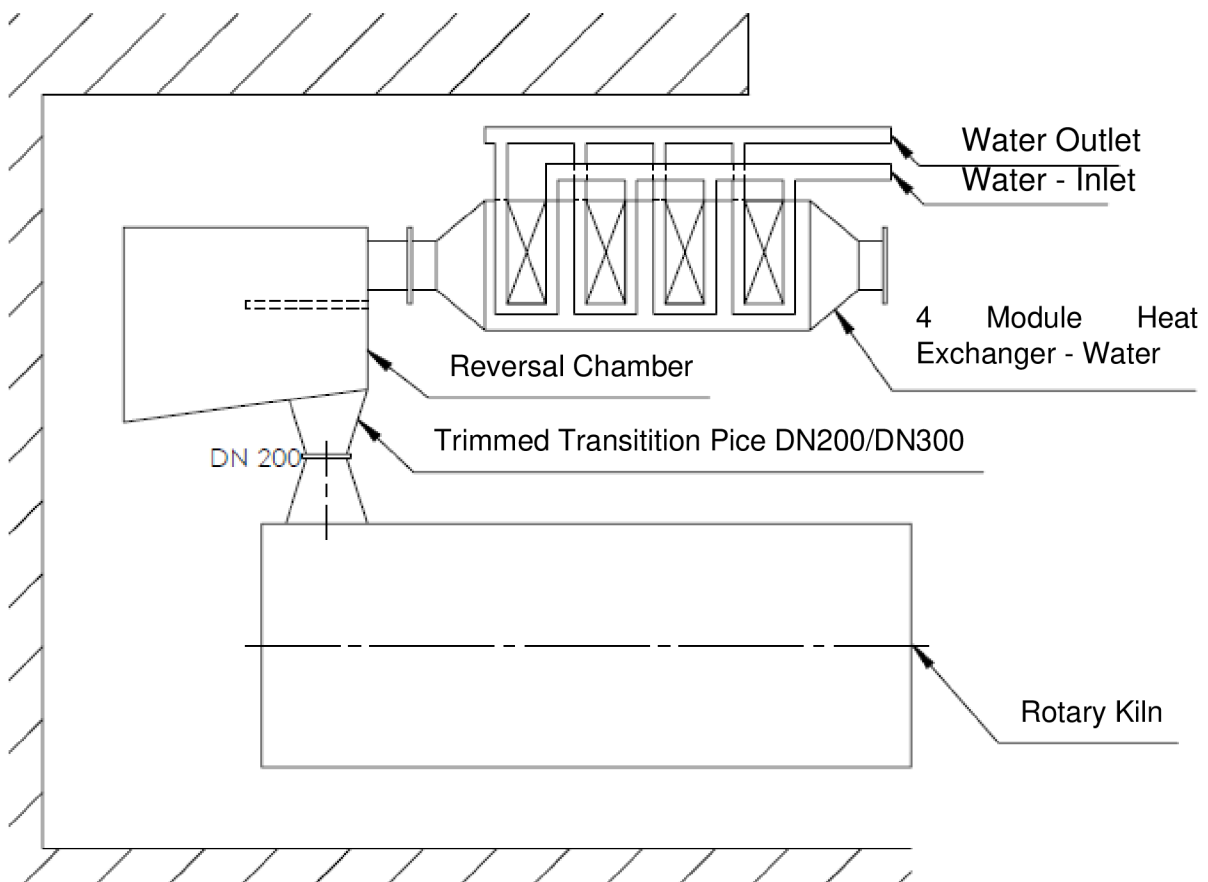


Figure 14: Future situation at the research furnace

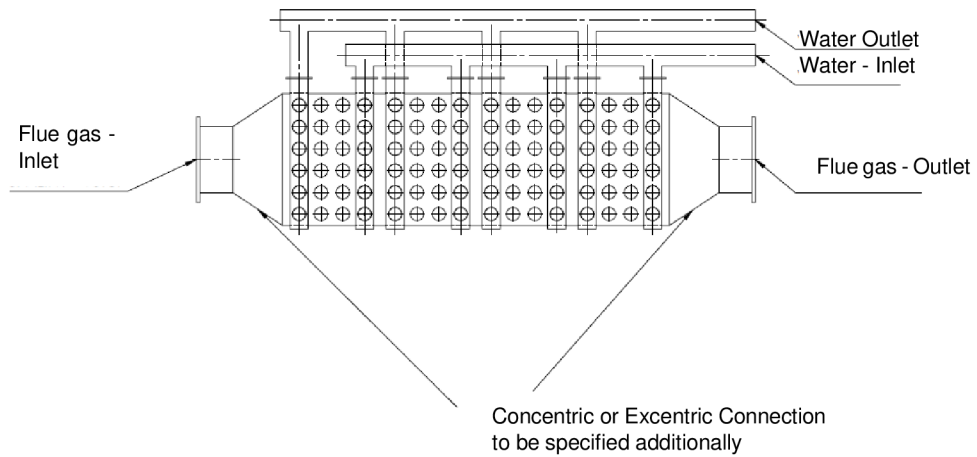


Figure 15: Sketch future modular heat exchanger

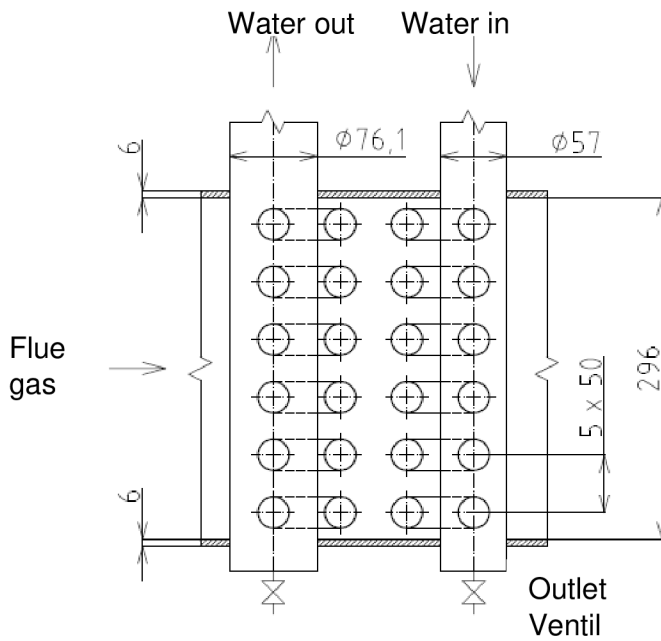


Figure 16: Water distribution and collection for one module

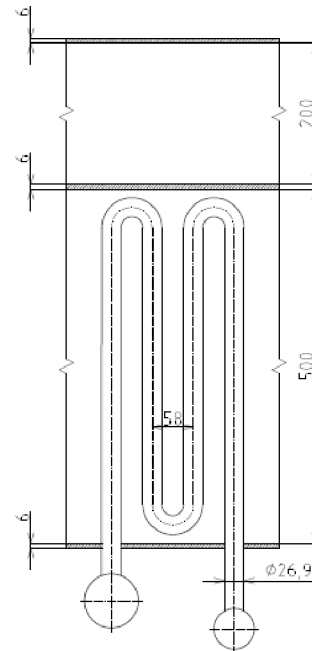


Figure 17: Serpentine of one heat exchanger tube

2.2 Thermal-hydraulic design of modular heat exchanger using HTRI Xchanger Suite

HTRI Xchanger Suite is a program to rate and design heat exchangers. For the thermal hydraulic design, the *Case Mode Simulation* is to use and the fluids and their properties, like the mass flow rate and inlet temperatures, must be entered in the software form. Furthermore, the *Unit type*, as well the *Orientation* of the heat exchanger and the location of the hot fluid have to be specified. Thereafter, the measurements, form and orientation of the tubes are required. (Figure 18)

Case Mode
 Rating Simulation Classic design Grid design

Process Conditions

Flow rate	Hot Outside	<input type="text" value="0,231"/>	kg/s	Cold Inside	<input type="text" value="1,3858"/>	kg/s			
Inlet/outlet Y	<input type="text" value="1"/>	/	<input type="text" value="1"/>	wt. frac. vapor	<input type="text" value="0"/>	/	<input type="text" value="0"/>	wt. frac. vapor	
Inlet/outlet T	<input type="text" value="950"/>	/	<input type="text"/>	C	<input type="text" value="20"/>	/	<input type="text"/>	C	
Inlet P/Allow dP	<input type="text" value="101"/>	/	<input type="text"/>	kPa	/	<input type="text" value="600"/>	/	<input type="text"/>	kPa

Unit Geometry

Unit type	<input type="text" value="Economizer"/>	Number of bays in parallel per unit	<input type="text" value="1"/>
Orientation	<input type="text" value="Horizontal"/>	Number of bundles in parallel per bay	<input type="text" value="1"/>
Hot fluid	<input type="text" value="Outside tubes"/>	Number of tubepasses per bundle	<input type="text" value="4"/>
Apex angle	<input type="text"/>	deg	

Tube and Bundle Geometry

Type	<input type="text" value="Plain"/>	Wall thickness	<input type="text" value="2,3"/>	mm	
Length	<input type="text" value="0,4"/>	No. of tuberows	<input type="text" value="4"/>		
OD	<input type="text" value="26,9"/>	No. of tubes in odd/even rows	<input type="text" value="6"/>	/	<input type="text" value="6"/>
Transverse pitch	<input type="text" value="50"/>	Tube form	<input type="text" value="Serpentine"/>		
Longitudinal pitch	<input type="text" value="58"/>	Tube layout	<input type="radio"/> Staggered	<input checked="" type="radio"/> Inline	

Figure 18: HTRI Xchanger Suite: Input summary

With measurements and orientation of the tubes, *the length, wall thickness, number of passes*, the *longitudinal* and *transversal pitch* are meant. Additionally, the *tube material* or *thermal conductivity* and eventual special shapes or internals are to specify in HTRI as well. The values and description of the pitch measurements can be seen in Figure 19.

Tube Geometry

Tube type: Plain

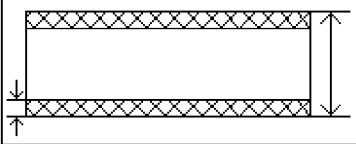
Tube internals: None

Tube material code: Carbon steel

Tube thermal conductivity: W/m-C

Wall thickness: mm

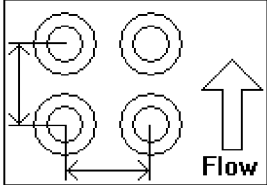
Tube OD: mm



Pitch

Equilateral layout

Longitudinal pitch: mm



Transverse pitch: mm

Figure 19: HTRI Xchanger Suite: tube geometry

Once the tubes are described, the bundle must be described. Therefore, the *bundle type*, tube form, number of tube rows / passes and tubes in odd/even rows and the *tube layout* must be entered. The values are to see in Figure 20.

Air Cooler and Economizer Tube

Default bundle type: Rows

Number of tuberos / tubepasses: /

Tubes in odd/even rows: /

Tube form: Serpentine

Clearance, wall to first tube: mm

Tube layout: Staggered Inline

Bundle width: m

Ideal bundle: Yes No

Tube Length

Tube length: m

Additional unheated length: mm

Unfinned tube length: mm

Equivalent tube length in tube bends for U-tubes: m

Stream Analysis

Use stream analysis: Yes No

Seal strip clearance: mm

Pairs of seal strips: Program Set

Seal strip width: mm

Figure 20: HTRI Xchanger Suite: bundle geometry

After entering all the required parameters the flow arrangement output (Figure 21) of the HTRI software can be compared to the actual design, in order to doublecheck if the arrangements are congruent and therefore the entered data should bring useful results.

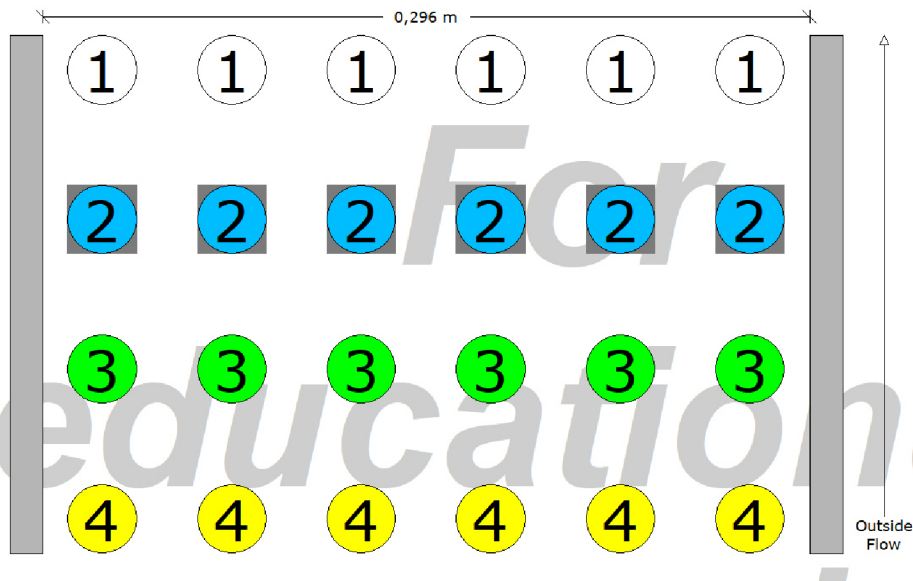


Figure 21: HTRI Xchanger Suite: tubes of one tube bundle / module

As the heat exchanger is modular, the simulation was performed for each section or module separately, using the output data from the previous section as input data for the following. This does not only make sense due to the fact, that more data about the heat exchanger is collected, but is necessary to get a more representative simulation result. In between the modules the spacing of the tubes is bigger and thus the flow would not be the same as in a single bigger bundle. Else this gives values to compare with the later following CFD simulation results.

A summary of the input parameters, were used for the HTRI simulation, is given in Table 1, Table 2 and Table 3.

Table 1: HTRI Input A

Fluids	Flow rate [kg/s]	Inlet temperature [°C]	Unit Type	Orientation
Hot outside	0,231	950	Economizer	Horizontal
Cold inside	1,3858	20		

Table 2: HTRI input B

Tubes	Nr. Passes per bundle	No. Of Rows in odd/even rows	Form	Layout	Type	Material	Outer diameter	Wall thickness
Parameter	4	6 / 6	serpentine	Inline	plain	Carbon steel	26,9 mm	2,3 mm

Table 3: HTRI input C

Shell	Tube length in gas stream per pass	Tube pitch longitudinal	Tube pitch Transversal	Wall clearance
Parameter	0,458 m	58 mm	50 mm	9,55 mm

As HTRI uses only the straight part of the serpentines for the heat exchange simulation. This is due to the fact, that most industrial economizers have the tube bends outside the flue gas flow. To compensate for that the set to 458 millimeters. This equals the measurement from one middle line of a serpentine to another one and was calculated by adding two times the bend radius to the straight section. Even if this is just an approximation it accounts for a bigger heat exchange area and a greater cross section for gas flow. As the heat exchange area on the outside of the bend is greater, the area on the inside is less, which should about even out. As for the flue gas cross section the length of 458 millimeter still is less than the actual given. Nonetheless using the actual cross section would probably lessen the pressure drop by to far, as the bends within the flow will cause additional turbulences. Furthermore, as the temperature changes in the gas are quite high, an extra simulation for the gas turbulences might cause more confusion than giving better results. The additional pressure drop due to the longer calculated straight part is acceptable, as it doesn't exceed the relatively long tubing from the distributor and collector into and out of the heat exchange area, but compensates for the unconsidered length of this tube part.

The simulations were performed twice, once without a fouling resistance and once with a fouling resistance of 0,00017 m²*K/W for City or Well Water on the tube side [5, p. 81] and a fouling factor of 0,0018 m²*K/W for Diesel or Natural Gas Combustion on the shell side. [5, p. 82].

2.3 Main design results

The output values of the HTRI simulations are listed in Table 4 and Table 5. Outlet 1, 2, 3 and 4 are the values after each of the 4 heat exchange modules. For the gas (i.e. air) stream a total difference was calculated, for comparison with the target values, as the effects of each module add up. The target values for the water streams were averaged, as an even distribution of water over the four modules is assumed and thus an average of temperatures and pressure drop is to be expected.

Table 4: Results HTRI simulation - Air / Gas

Air / Gas	Value [Unit]	Inlet	Outlet 1	Outlet 2	Outlet 3	Outlet 4	Total Diff.	Target
HTRI without Fouling	T [°C]	950	780,28	643,81	532,46	442,38	-507,62	[-500; -490]
	p [kPa]	101	100,98	100,96	100,94	100,93	-0,07	>= -0,100
HTRI with Fouling	T [°C]	950	796,21	669,17	563,04	475,33	-474,67	[-500; -490]
	p [kPa]	101	100,98	100,96	100,94	100,93	-0,07	>= -0,100

Table 5: Results HTRI simulation - water

Water	Value [Unit]	Inlet	Outlet 1	Outlet 2	Outlet 3	Outlet 4	Average Diff.	Target
HTRI without Fouling	T [°C]	20	27,81	26,12	24,88	23,88	5,67	<=10
	p [kPa]	600	598,89	598,88	598,88	598,87	-1,12	>= -1
HTRI with Fouling	T [°C]	20	27,08	25,72	24,68	23,80	5,32	<=10
	p [kPa]	600	598,89	598,88	598,88	598,87	-1,12	>= -1

The results show that the modular heat exchanger without considering fouling exceeds the requirements regarding the heat duty by about 1 %. The pressure drop on the gas side is within the range, wished for. The pressure drop of one kilo Pascal for just the serpentine is given too, regarding the accuracy of given didges for the allowed pressure drop.

Neglecting the thickness of the fouling layers, the pressure drops for the simulations with fouling remain the same. The heat duty for a fully build up fouling layer lays about 4 % below the required heat duty. Still the range in which the heat exchanger operates is in the building phase of the fouling, as this phase is to be researched. Thus, the heat exchanger is well designed, according to the results of the HTRI simulations.

3 Analysis of uniformity of water distribution inside one tubular module of heat exchanger

As next step of evaluating the design of the Modular Heat Exchanger, the uniformity of the water distribution towards the heat exchanger pipes in a module is numerically simulated. Due to manufacturing reasons some design changes occurred in comparison with the in HTRI simulated version, the CFD simulation was performed with the latest available model. For the simulation, the academic version of *Ansys Workbench 20019 R3* was used. The flow distribution analysis included the process of generating a CAD model, choosing a suitable viscosity model and solution methods. Setting suitable initial and boundary conditions in order to mimic the operation conditions and a high-quality mesh are also required to run the simulation successfully and get reasonable results.

3.1 Creation of a model for CFD simulation

As mentioned above, for the final version of the modular heat exchanger a few changes in comparison with the primary design were made. The main differences are that in the final version the distributor pipe is closer to the heat exchanger shell than the collector pipe while the flow direction of the water and the tube pitch remain the same. The straight part of the serpentine was shortened to 375 mm and the pipe diameters changed to the ones listed in Table 6.

Table 6: Tube dimensions - final design

Tube	Inner Diameter [mm]	Thickness [mm]	Outer Diameter [mm]	DN
Distributor	53,9	3,2	60,3	50
Collector	68,9	3,6	76,1	65
Serpentines	21,1	2,9	26,9	25

Further dimensions can be seen in Figure 22: Top View of Heat Exchanger Module

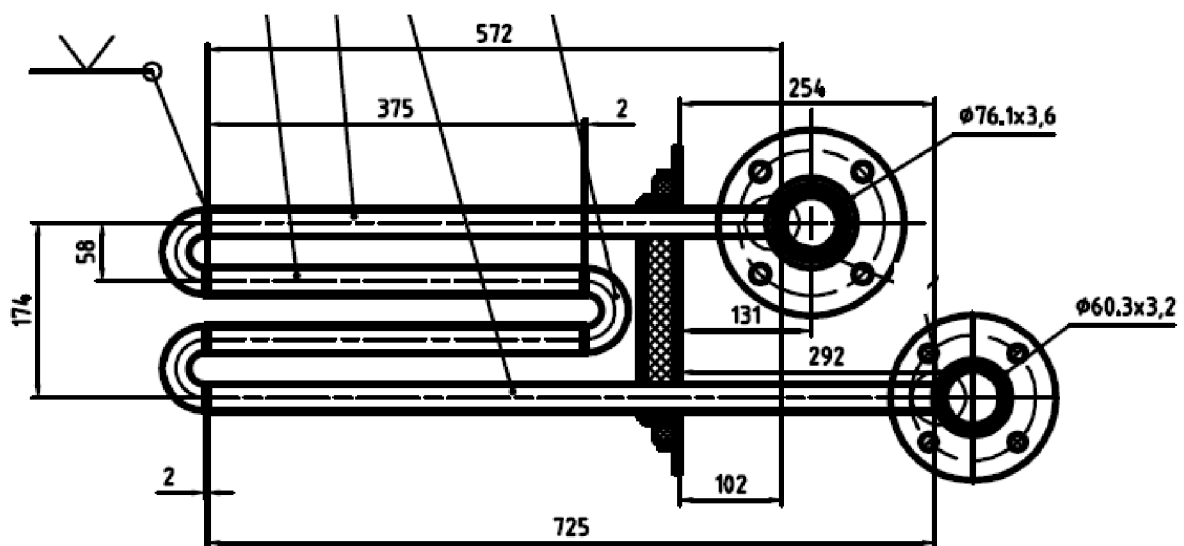


Figure 22: Top View of Heat Exchanger Module

3.1.1 Geometry

For the CFD simulation the inner space of one heat exchanger module was modelled in *Ansys Space Claim*. Therefore, the tube path of one serpentine was sketched. On the ends of the tube paths circles with the inner diameters of the distributor and collector were added into the same plane. The inner diameter circle of the serpentine was placed in the plane normal to straight parts of the serpentine. Then the body of the first serpentine was modeled by sweeping the inner diameter over the tube path. The serpentine was multiplied by a linear 6 x 50 mm linear pattern. Thereafter the distributor and collector were extruded, and all the bodies were merged. After creating the needed cutting planes the tubes were cut into pieces, in order to create surfaces for monitoring the mass flow rates of each tube and more possibilities to adapt the mesh. The main cuts were placed where the serpentine enters the inner side of the heat exchanger shell and 3,8 mm away from the collector and distributor pipes, which allows for smooth mesh transitions. The monitoring surfaces were created in the cut of the last straight part of the serpentine. Further cuts were made to separate the fluid body for more specific meshing. For example, the sweepable start and end pieces of the collector and distributor were created in order to get a better cell quality and fewer cells in total. To get matching faces during meshing the geometry setting *share topology* was set to *share*.

3.1.2 Mesh and numerical model

For a mesh there are several parameters that have a major impact on the simulation results. These also depend on the model that is chosen for simulation. However, to be economic in terms of calculation resources and to keep the cell count within the limit of the student license of 512000 cells, some compromises had to be made. Those will be pointed out when they happen to occur and interfere with the desired mesh attributes.

Due to the flow regime and the geometry the turbulence model of first choice was *Shear-Stress Transport (SST) k- ω Model* which, for this geometry, has an advantage over the standard and the BLS k- ω Model as it accounts for the transport of the turbulence shear stress in the definition of the turbulent viscosity and thus is better in predicting the flow separation of viscous fluids from smooth surfaces.

To solve the viscous layer at the boundaries the mesh needs to be fine enough. This means that the dimensionless cell height y^+ needs to be determined and the *First Layer Thickness* for the *Inflation* on the walls needs to be adapted in accordance. For the k- ω model, the y^+ value at the walls is recommended to be kept under 5 [6]

The y^+ value can be calculated from the cell height, the shear stress velocity and the dynamic viscosity (60).

$$y^+ = y \cdot \frac{w_\tau}{\nu} \tag{60}$$

With:

ν	[m ² /s]	Kinematic viscosity
w_τ	[m/s]	Shear stress velocity
y^+	[-]	Dimensionless wall distance
y	[m]	Wall distance

The initial first layer thickness was estimated according to the formulas of Table 8.1 in the book Centrifugal Pumps [7, p. 551]. For a y^+ value of 1, the estimated *First Layer Thickness* would be $0,6 \times 10^{-5}$ m. This value was primarily used for the small k- ω mesh, as the y^+ value was to be below 5.

The global settings for the k- ω mesh are to be seen in

Figure 23 and the applied methods are summarized in Table 7. The *Element Size* is set to 7 mm while the allowed *Maximum Size* is 12 mm. The *Growth Rate* is with a value of 1,2 set to default and *Capture Curvature* is activated. In order to get better cells in the critical regions where the stream leaves or enters the distributor or collector, the *Target Skewness* is set to 0,65. This value as well as most of the others were found in an iterative process of trial and error, with the aim of finding a balance between good cell quality and a low number of elements. As the maximum allowed number of elements for the commonly available license is 512000, with a total number of 507829 elements the room to adapt the mesh even further is very small.

The high cell count of the mesh is the reason why further adaptation of the mesh to get rid of y^+ values that exceed five was not possible. However, the vast majority of cells (96,4 %) on the walls have y^+ values below 5,0. **Error! Reference source not found.** illustrates that with the histogram of the y^+ distribution in blue and the cumulative percentage in orange. Still, the cells which exceed the value of 5,0 are in the critical region where the serpentes connect. That is the reason why another approach to evaluate the results was needed.

<input type="checkbox"/> Display			
Display Style		Use Geometry Setting	
<input type="checkbox"/> Defaults			
Physics Preference		CFD	
Solver Preference		Fluent	
Element Order		Program Controlled	
<input type="checkbox"/> Element Size		7, mm	
Export Format		Standard	
Export Preview Surface Mesh		No	
<input type="checkbox"/> Sizing			
Use Adaptive Sizing		No	
<input type="checkbox"/> Growth Rate		1,2	
<input type="checkbox"/> Max Size		12, mm	
Mesh Defeaturing		Yes	
<input type="checkbox"/> Defeature Size		Default (3,5e-002 mm)	
Capture Curvature		Yes	
<input type="checkbox"/> Curvature Min Size		Default (7, e-002 mm)	
<input type="checkbox"/> Curvature Normal Angle		Default (18,°)	
Capture Proximity		No	
Bounding Box Diagonal		955,74 mm	
Average Surface Area		7526,9 mm ²	
Minimum Edge Length		66,288 mm	
		<input type="checkbox"/> Quality	
		Check Mesh Quality	Yes, Errors and Warnings
		<input type="checkbox"/> Target Skewness	0,65
		Smoothing	High
		Mesh Metric	Aspect Ratio
		<input type="checkbox"/> Min	1,0717
		<input type="checkbox"/> Max	1,5293e+007
		<input type="checkbox"/> Average	1141,9
		<input type="checkbox"/> Standard Deviation	1,1096e+005
		<input type="checkbox"/> Inflation	
		<input type="checkbox"/> Assembly Meshing	
		<input type="checkbox"/> Advanced	
		<input type="checkbox"/> Statistics	
		<input type="checkbox"/> Nodes	1878178
		<input type="checkbox"/> Elements	507829

Figure 23: Global settings and properties of small k- ω mesh

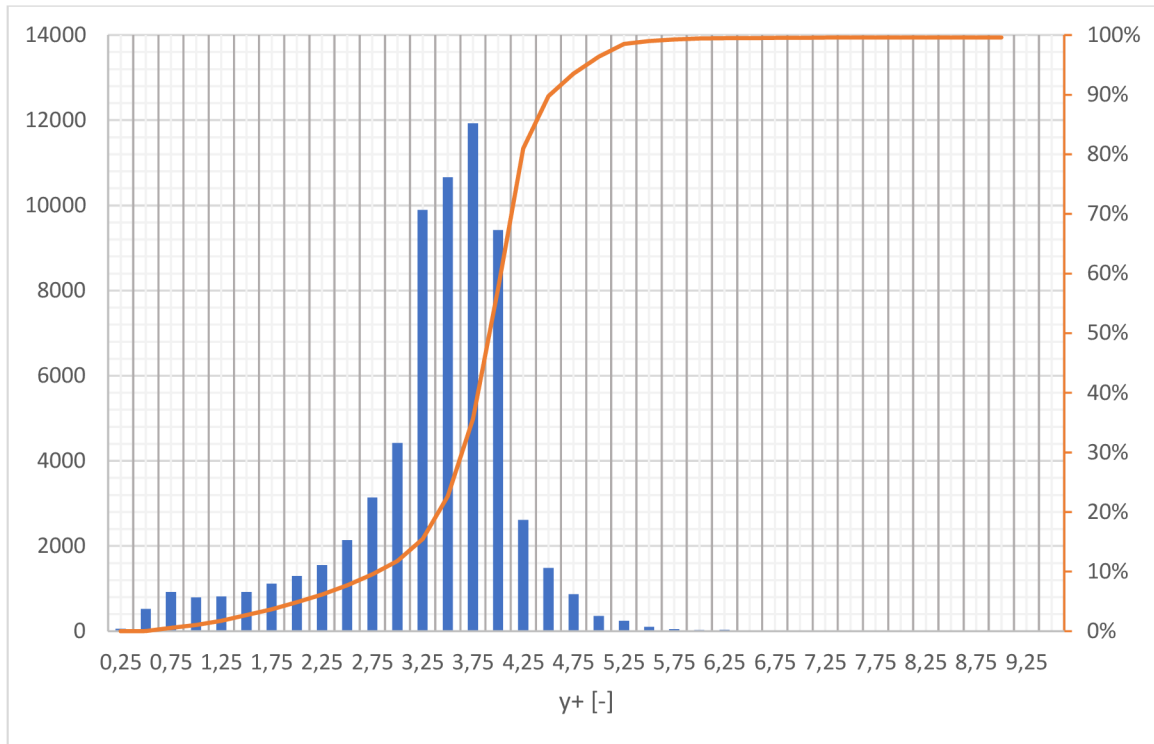


Figure 24: Histogram elements - y^+ with curve of cumulative percentage

Table 7: Used methods and settings for k- ω mesh

Method	Part	Bodies	Faces	Edges	Size [mm]	Layers	activated features
Inflation	Collector and Distributor	6	8		0,02	5	first layer thickness
Inflation	Serpentines	30	72		0,014	5	first layer thickness
Multizone	Collector and Distributor Top and Bottom	4			7		
Sizing	In- and Outlet Top and Bottom		4		5,6		
Multizone	Serpentines in and out flow parts	12			4		
Multizone	Serpentines Bends and inner straight parts	6			5,6		
Multizone	Serpentines straight part after monitors	6			6		
Edge sizing	Serpentine Circumference			12	18 Divisions		

The different *Multizones* and *Sizings* were chosen to get smooth transitions of the mesh with appropriate mesh density for each part of the geometry. (Figure 25).

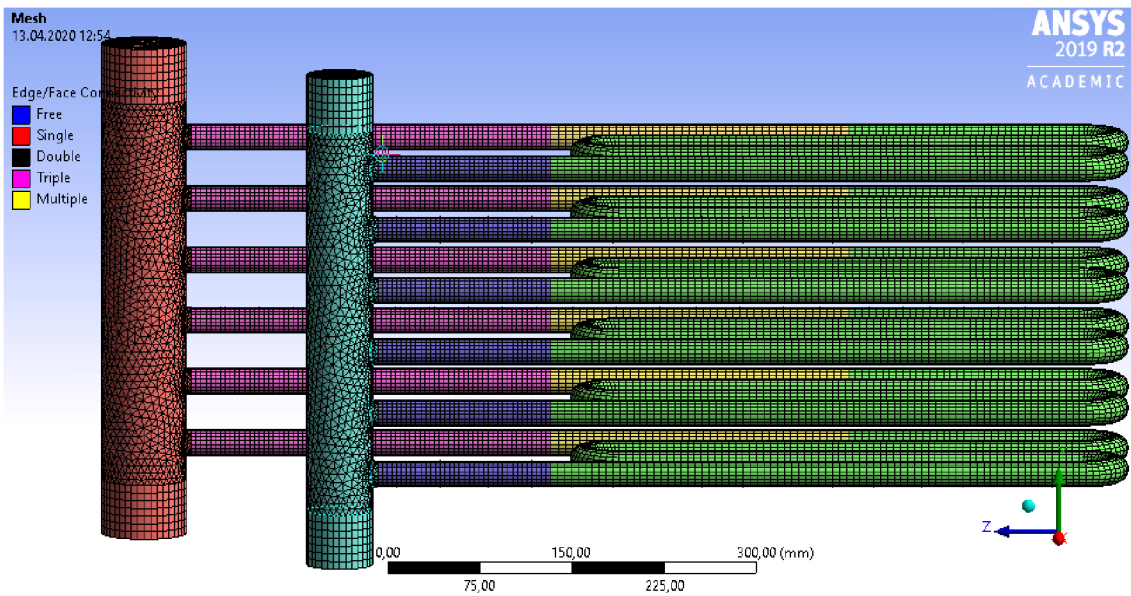


Figure 25: Meshed geometry with colored regions

To obtain the needed First Layer Thicknesses a few simulation runs and adaptations were necessary to follow the listed requirements ($y^+ < 5$ and maximum cell count). In the final mesh a five-layer inflation on all walls was applied. In distributor and collector, the first layer has a height of 0,020 mm (Figure 26) while in the serpentine the height is 0,014 mm (Figure 27).

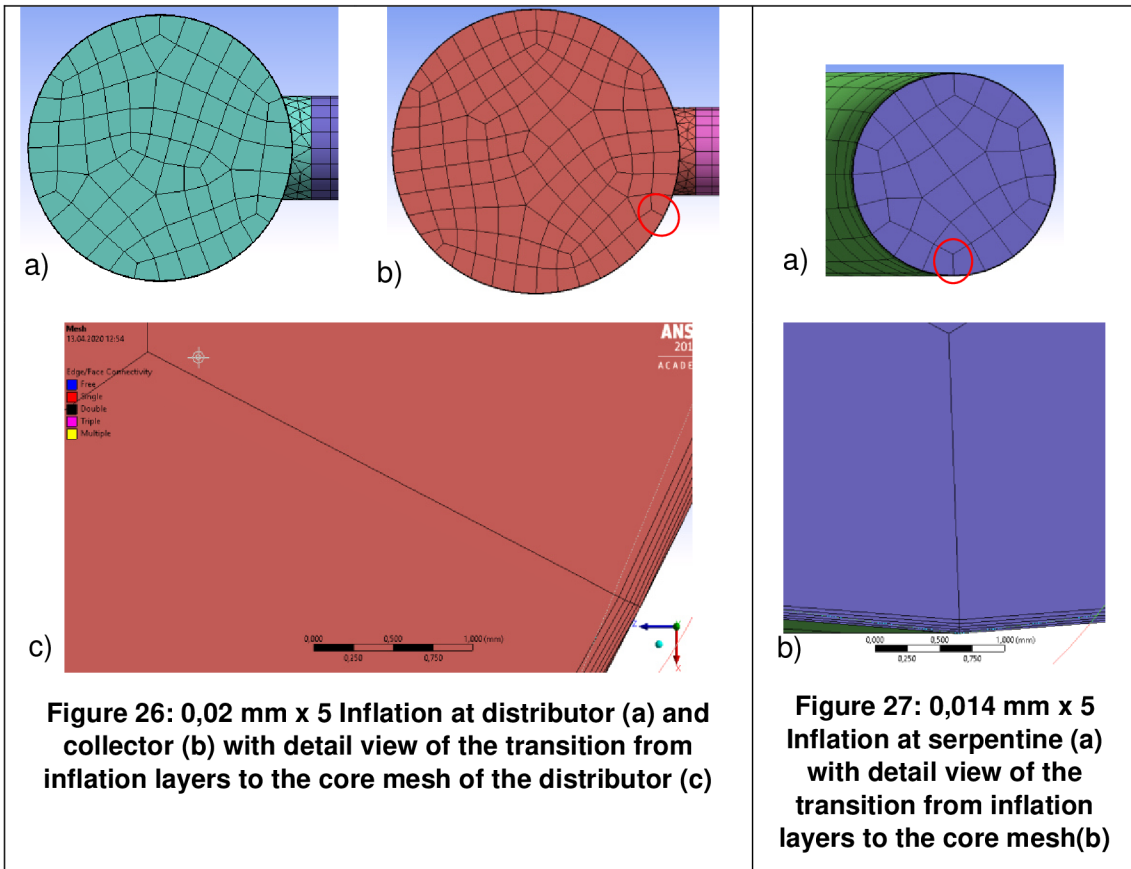


Figure 26: 0,02 mm x 5 Inflation at distributor (a) and collector (b) with detail view of the transition from inflation layers to the core mesh of the distributor (c)

Figure 27: 0,014 mm x 5 Inflation at serpentine (a) with detail view of the transition from inflation layers to the core mesh(b)

The *Mesh Metrics* are to find in Table 8. The mesh quality is quite high, as especially the *Average Skewness* of 0,19548 and the *Orthogonal Quality* of 0,80586 indicate. Even though the *Maximum Skewness* lies at 0,73649 which is acceptable, the location of the highly skewed cells is rather inconvenient. As to see in Figure 28 most problematic cells are to find around the entrance and the exit of the heat exchange pipes. This might influence the simulation of the stream and the stability of the simulation. The y^+ values are illustrated in Figure 29. The red areas are the most turbulent regions, but as the y^+ values did not decrease with a decrease of the layer thickness of the inflations, calculation errors may have occurred. These may be caused by two factors. First are the problematic cells in the region. Second is the big jump in cell size from the inner mesh to the inflation layers at the walls, as to see in Figure 26 and Figure 27. The high maximum *Aspect Ratios* occur in the straight parts of the pipes, where longer cells were used. This should not harm the accuracy of the simulation, as the cells are stretched in the direction of the flow.

Table 8: Element metrics of small k- ω mesh

Mesh Metrics	Average	Standard deviation	Minimum	Maximum
Element Quality	0,29202	0,38706	0,00356	0,99998
Skewness	0,19548	0,10666	0,00158	0,73649
Aspect Ratio	1141,9	110960	1,0717	15293000
Orthogonal Quality	0,80586	0,21842	0,0142	0,99972

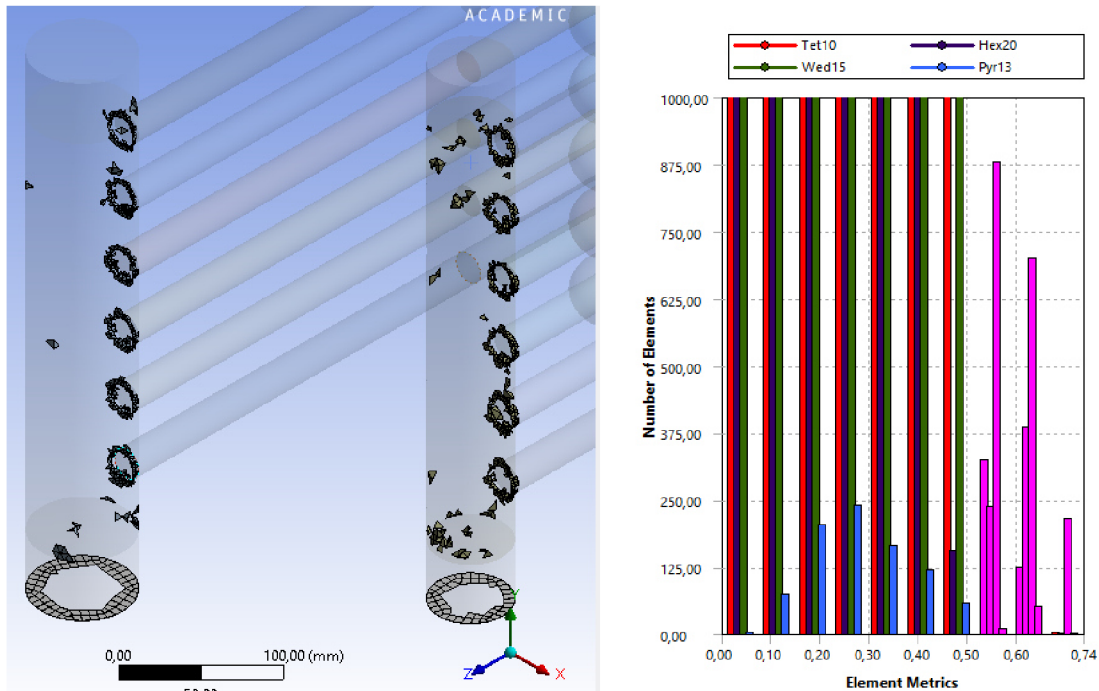


Figure 28: Skewed cells of the small k- ω mesh (skewness > 0,5)

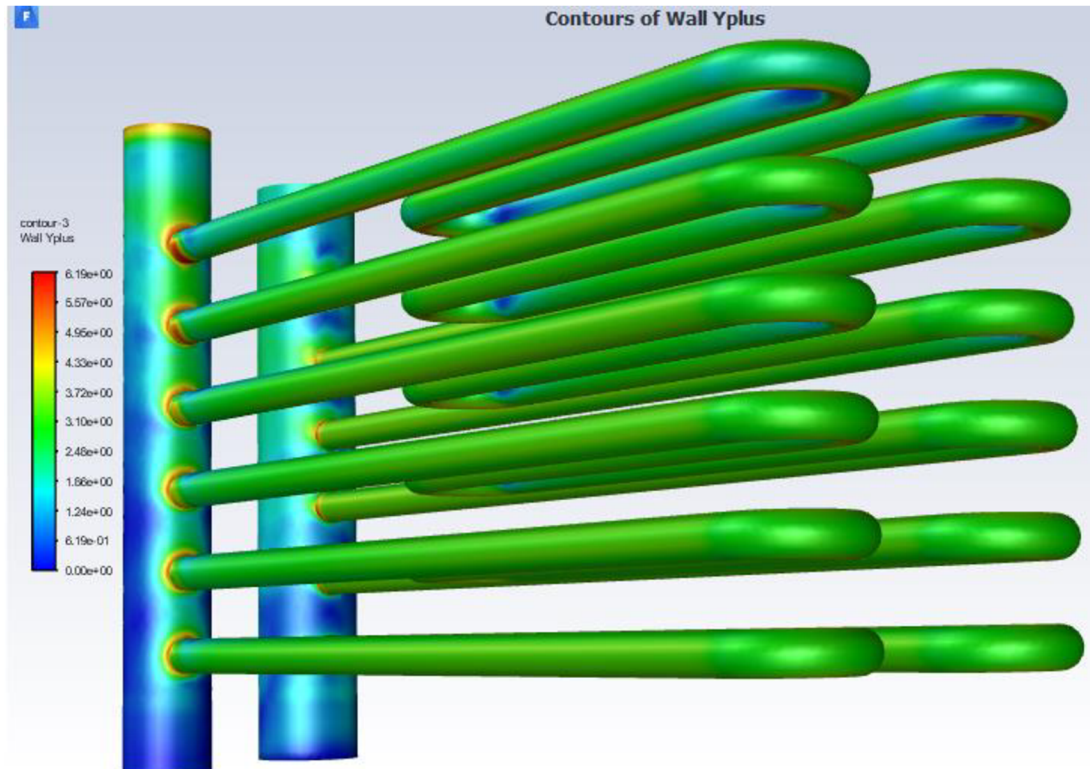


Figure 29: Contour plot - y^+ values of the small $k-\omega$ model (Scale [0; 6,19])

Cells of problematic quality and too high y^+ values might skew simulation results. To give a reference whether the solution acquired with the limited cell count of the academic version is representative or not, a simulation with the same geometry and a significantly bigger mesh was simulated in collaboration with Mrs. Dominika Fialová from UPI VUT Brno. The number of its cells is 4259698, which is about 8 times the limit of the student ANSYS version. The high number of cells is a result of smaller cells in general (i.e. smaller *Maximum Size* and smaller set *Element Size*) and of the 24 inflation layers, which hugely contribute to the higher cell count. However, the high number of inflation layers is necessary to get less of a jump from the core mesh to the inflation layer and to cover the whole viscous layer of the wall with the inflation. The y^+ values for this mesh are under 5, which proves the thesis that the sudden jump from the core mesh to the inflation layer on the small mesh was at least part of the problem causing the y^+ values staying too high. The main mesh settings remain similar to the other $k-\omega$ mesh, except for an element size of 4 mm and a *Target Skewness* of 0,6.

The other applied meshing methods can be seen in Table 9. In addition to that the first cell distance was further adapted in Fluent. As a result of the adaptation cells, in the most turbulent flow region at the walls were cut into more, smaller cells with half the thickness. Thus, the First Layer Thickness for those cells resulted at about 0,0035 mm.

Table 9: Mesh set up big k- ω mesh

Method	Part	Bodies	Faces	Edges	Size [mm]	Layers	activated features
Inflation	Collector and Distributor Top	2	2		0,00830	24	first layer thickness
Inflation	Collector and Distributor Midsection	2	2		0,007	24	first layer thickness
Inflation	Collector and Distributor Bottom	2	2			24	Smooth transition
Sizing	In- and Outlet		2		2,3		
Inflation	Serpentines	26	72		0,007	24	first layer thickness
Sizing	Serpentines		6		1,90		
Multizone	Collector and Distributor Top	2			4		
Multizone	Collector and Distributor Bottom	2			default		
Multizone	Serpentines flow parts	6	6		2		
Multizone	Serpentines Bends and inner straight parts	6	6		4		
Multizone	Serpentines after the monitors	6	6		4		
Multizone	Serpentines out flow	6	6		2		
Edge sizing	Serpentine Circumference			12	30 Divisions		

Figure 30 and Figure 31 show the faces of the inlet and one serpentine pipe, respectively. The difference of the transition from the inflation to the core in comparison with the transition at the small k- ω mesh is quite significant. The overall element metrics for this mesh are listed in

Table 10. If one compares the skewed cells between the big and the small k- ω mesh, one might find that the location of the most problematic cells match (see Figure 28, Figure 32).

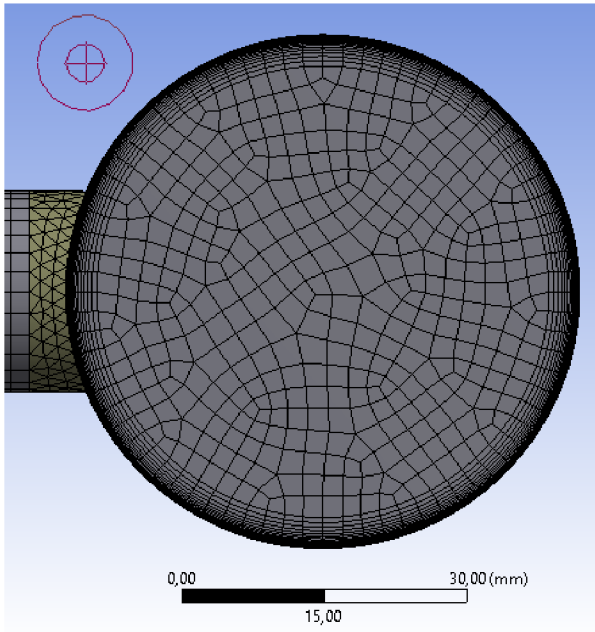


Figure 30: 0,0083 mm x 24 Inflation at collector

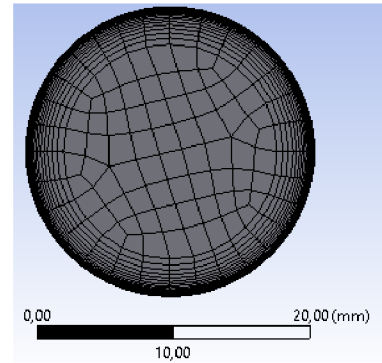


Figure 31: 0,007 mm x 24 Inflation at serpentine

Table 10: Mesh Metrics - big k- ω mesh

Mesh Metrics	Average	Standard deviation	Minimum	Maximum
Element Quality	0,15067	0,242	0,00175	1
Skewness	0,15242	0,0987	0,000845	0,72052
Aspect Ratio	150,34	7922,5	1,0766	3930000
Orthogonal Quality	0,89742	0,14977	0,0337	0,99993

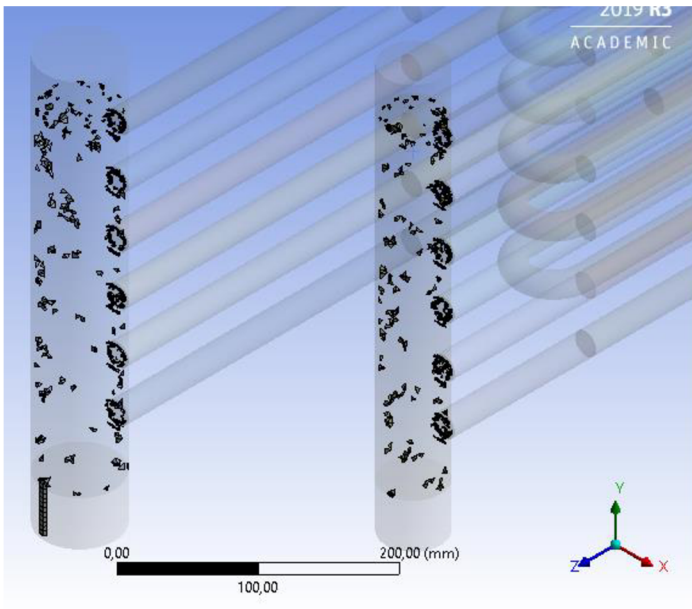
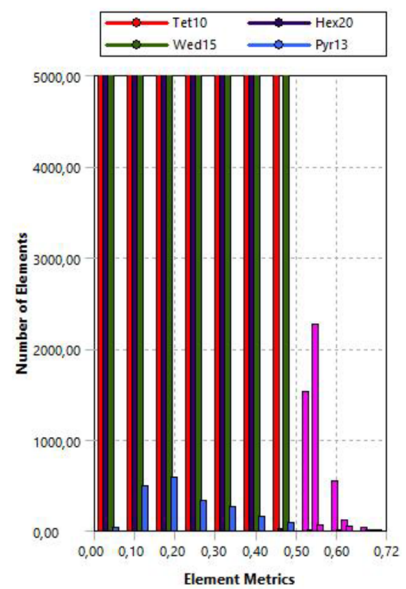


Figure 32: Skewed cells of the big k- ω mesh (skewness > 0,5)



To get a valid solution with the student license a second approach was taken. The $k-\varepsilon$ – *Realizable Model* with the *Non-Equilibrium Wall Function* was chosen for the second approach. The $k-\varepsilon$ – realizable model is the second option for simulating standard cases, where turbulent interaction with the wall is of importance. If a wall function is used a mesh with a relatively thick first layer at the walls is needed. This allows for a smooth transfer from the outer mesh to the inner mesh, and requires less cells in total, for the same geometry. As the near field of the walls is not modelled in high resolution, the $k-\varepsilon$ is not suitable for temperature exchange simulations. However, for the investigation of the flow distribution it is sufficient. The term *realizable* means that the model satisfies certain mathematical constraints on the Reynolds Stresses, consistent with the physics of turbulent flows. This is important, as the flow in the serpentines is a fully developed turbulent flow ($Re = 13177 > 10^4$) [8].

According to the Ansys Theory Guide the Non-Equilibrium Wall Function requires y^* values bigger than 11,225 [9]. Any viscous layer in a region with a lower y^* value will be calculated with the lower limit of y^* , which is 11,225. The y^* is like the y^+ a dimensionless distance to the wall, which is dependent on the flow and the first layer thickness. The y^* calculates as follows:

$$y^* = y \frac{\left(\rho (C_\mu)^{\frac{1}{4}} (k_P)^{\frac{1}{2}} \right)}{\mu} \quad (61)$$

C_μ	[]	a function of the mean strain and rotation rates, the angular velocity of the system rotation, and the turbulence fields (k and ε)
ρ	[kg/m ³]	Fluid Density
μ	[kg/sm]	Dynamic Viscosity
k_P	[m ⁴ /s ²]	Calculation Constant
y^*	[-]	Dimensionless Wall Distance
y	[m]	Wall Distance

The $k-\varepsilon$ mesh was set up with the methods listed in Table 11 listed methods, and a slightly different geometry. The parts of the serpentines that connect to the distributor and the collector, and are part of the same bodies, are slightly longer in comparison with connection parts in the $k-\omega$ models. This change was made to prevent the accumulation of highly skewed cells in the middle of the tube mouth, which is one of the most critical parts of the flow and thus should be solved with a good quality mesh. It was found, that with more cells to generate the transition of the mesh from the bigger pipe into the smaller one, the meshing result is smoother and less skewed. The element size is set to 8 mm and the target skewness is 0,25. The thicker inflation layer allowed for the use of the *Sweep Method*. With the Sweep Method a *Sweep Bias* can be used to control the cell growth along the body, this method is applied to. It was used for an especially smooth transition from the fine mesh after the distributor to the mesh at the serpentines. So, after the automatic mesh of the distributor, a fine multizone meshed part follows, which's mesh transitions into a sweep mesh that ends into the coarser multizone mesh of the straight parts and the bends of the serpentines. As result the flow regions with the most turbulences could be simulated with minimal jumps in cell size.

Table 11: Mesh set up k-ε mesh

Method	Part	Bodies	Faces	Edges	Size [mm]	Layers	activated features
Inflation	Collector and Distributor	6	6		2,4	1	first layer thickness
Inflation	Serpentines	20	66		2,4	1	first layer thickness
Multizone	Collector and Distributor Top	2			6		
Multizone	Collector and Distributor Bottom	2			8		
Face Sizing	Inlet		1		5		
Multizone	First sections Serpentine	6			2,4		
Sweep	Second sections Serpentine	6					Bias 1,5 - - - -
Multizone	Serpentine Bends and inner straight parts	6			5,5		
Multizone	Serpentine straight part after monitors	6			3,6		
Edge sizing	Serpentine Circumference			12	24 Divisions		

Figure 33 and Figure 34 show the mesh faces of the Inlet and one serpentine, respectively. The transition from the inflation to the core mesh is quite smooth. The mesh quality of the k-ε mesh is slightly better than the quality of the k-ω mesh.

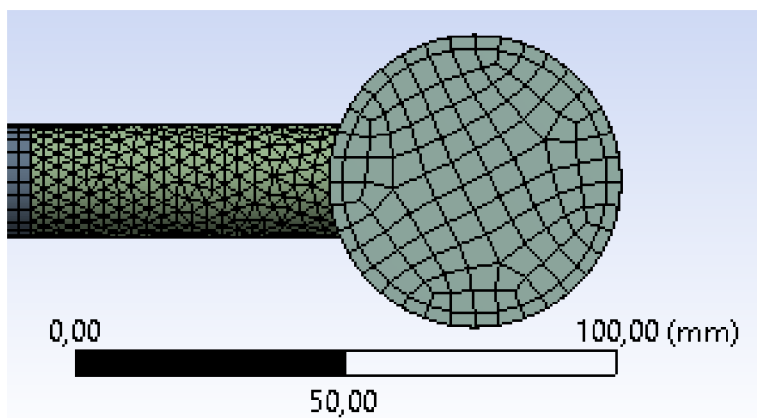


Figure 33: 2,4 mm x 1 Inflation at distributor

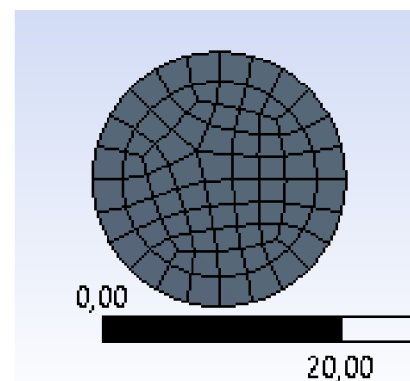


Figure 34: 2,4 mm x 1 Inflation at serpentine

The main difference is the better *Orthogonal Quality* of the k-ε mesh cells (Table 12). Furthermore the cells with a higher skewness than 0,5 are no longer located at the edges where the serpentine connects with the distributor and the collector, but only on the inflation layer directly after the connection in the serpentine (Figure 35).

Table 12:Element metrics of k-ε mesh

Mesh Metrics	Average	Standard deviation	Minimum	Maximum
Element Quality	0,71669	0,18522	0,24551	0,99999
Skewness	0,19729	0,1026	0,0185	0,71934
Aspect Ratio	2,2764	0,74357	1,0639	9,4376
Orthogonal Quality	0,9069	0,11716	0,28066	0,99981

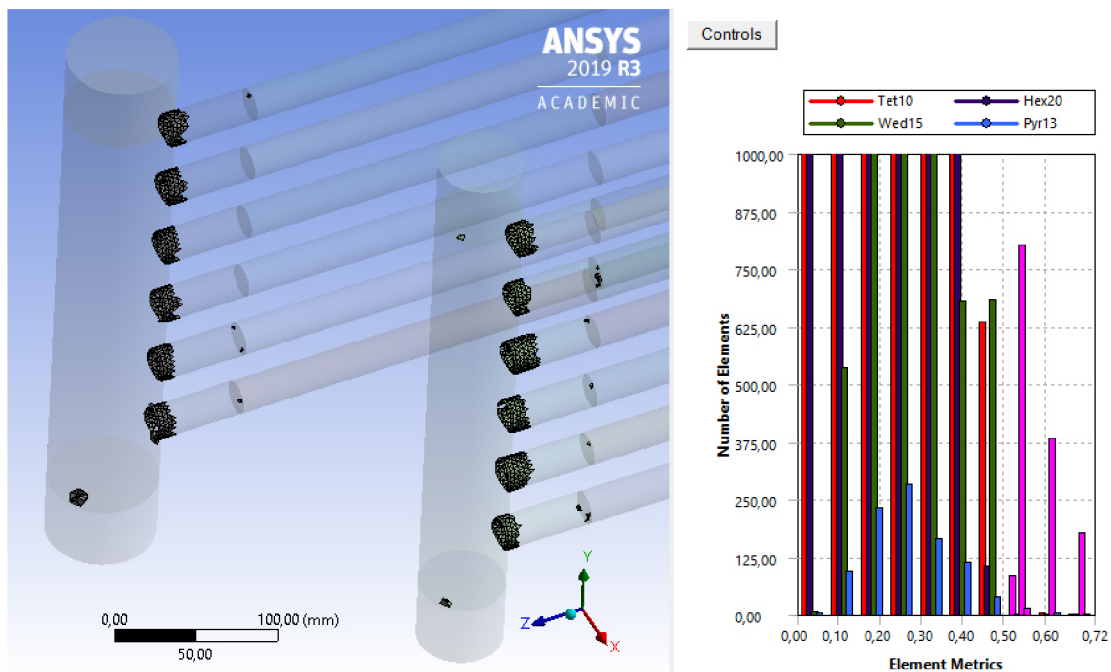


Figure 35: Skewed cells of the k-ε mesh (skewness > 0,5)

The y^* values of the mesh are mostly in the range as to be seen in Figure 36. They should be of a value higher than 11,225. 11,225 is the minimum value, that is used for modelling the viscous layer, even if the calculated value for this region is lower. But as there is zones where the flow velocity is very low, the y^* values in those regions get below the minimum recommended value. This will result in an insufficient emulation of a viscous layer. As the flow velocities are so low in those regions, the interaction with the wall there can be neglected to some degree. For the investigation of flow distribution, the most important regions are where the flow divides or collects. In those regions the flow velocity is not too low as to be seen Figure 37.

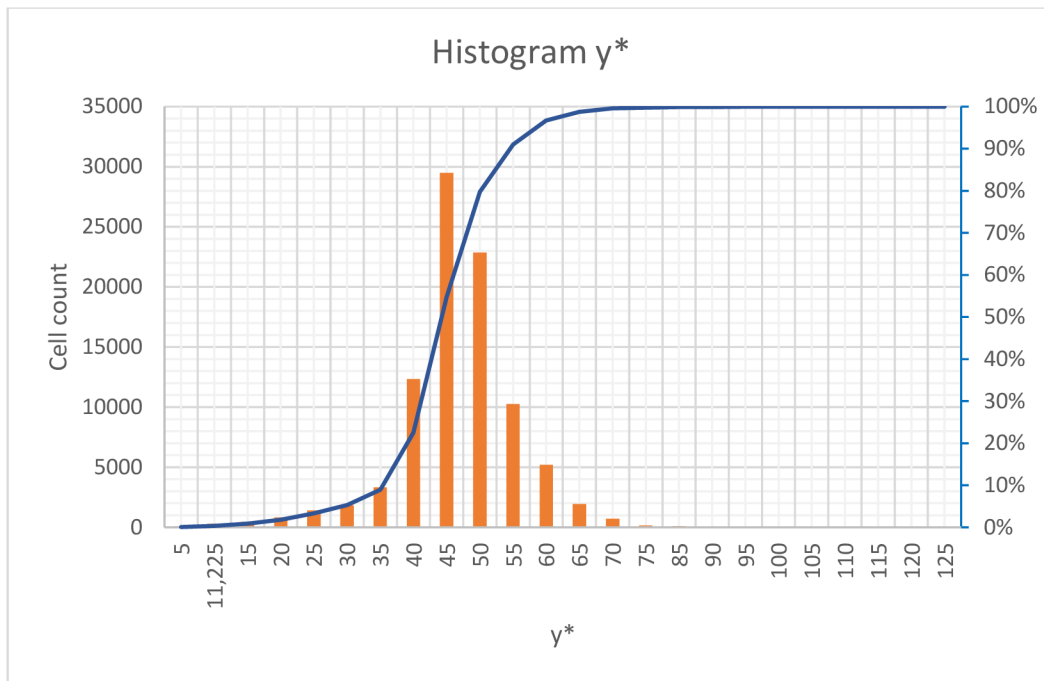


Figure 36: y^* -histogram of k- ϵ mesh with curve of accumulated percentages

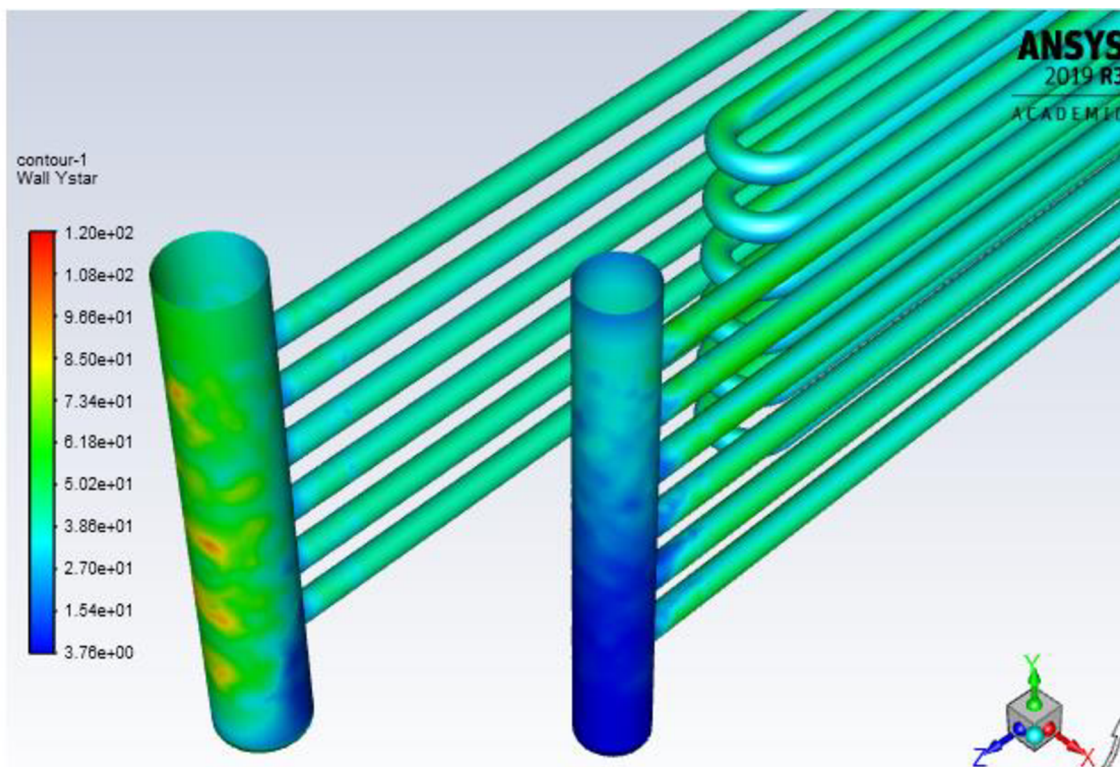


Figure 37: Contour plot – y^* values of the k- ϵ model

3.2 Setting of simulation conditions and run of simulation

To run the simulation successfully (i.e. to obtain accurate results) a viscosity model, that is compatible with the mesh and suits the problem, needs to be chosen. The rest of the settings deals with properties of the working fluid, boundary conditions, and solution methods so that the real fluid flow is simulated as good as possible. Table 13 and Table 14 show the settings of the three simulations that have been done. Settings, that are not listed or described were kept at default. The setting for *Energy* could be switched on, which resulted in an adiabatic simulation, or of which resulted in an isothermal simulation. In both cases there is no heat exchange with the environment, as no environment with any energy level was defined. The adiabatic simulation calculates the energy that is transformed into heat as a result of inner friction of the fluid and friction on the walls. This means extra computational effort. But it seemed to stabilize the simulation of the k- ω small mesh just enough to converge. Since there is no heat transfer a significant difference in the solution is not to expect.

Table 13: Simulation settings (1/2)

	k- ω small	k- ω big	k- ϵ
Solver Type	Pressure based	Pressure based	Pressure based
Time	Steady	Steady/Transient	Steady/Transient
Velocity Formulation	Absolute	Absolute	Absolute
Model	Viscous k- ω , SST	Viscous k- ω , SST	Viscous k- ϵ , Realizable
Wall Function	-	-	Non-Equilibrium
Options	Production Limiter		
Energy	Adiabatic (20 °C start)	Isothermal (20 °C)	Isothermal (20 °C)
Material	liquid-water	liquid-water	liquid-water
Boundary Conditions			
Inlet			
Reference Frame	Absolute		
Mass Flow Rate [kg/s]	1,386		
Direction Specification Method	Normal to Boundary		
Turbulence	Default		
Outlet			
Backflow Reference Frame	Absolute		
Gauge Pressure	0		
Pressure Profile Multiplier	1		
Backflow Direction Specification Method	Normal to Boundary		
Backflow Pressure Specification	Total Pressure		
Wall			
Wall Motion	Stationary		
Shear Condition	No Slip		
Roughness Model	Standard		
Roughness Height [mm]	0,15		
Roughness Constant	0,5		

Table 14: Setting of the Solution Methods (2/2)

	k- ω small	k- ω big	k- ϵ
Methods			
Scheme	SIMPLE		
Gradient	Green-Gauss Node Based		
Pressure	Second Order		
Momentum	Second Order Upwind		
Turbulent Kinetic Energy	Second Order Upwind		
Specific Dissipation Rate	Second Order Upwind		
Energy	Second Order Upwind		
Transient Formulation	-	Second Order Implicit	First Order Implicit
Controls	Default		
Convergence Criteria - Residuals			
Continuity	0,001	0,000001	0,001
X-velocity	0,001		
Y-velocity	0,001		
Z-velocity	0,001		
k	0,001		
ϵ			0,001
ω	0,001	0,001	

To control how steady the results are, control points were added into the turbulent areas of the distributor and first serpentine (Figure 38). Once the *Facet Average Velocity* in those points did not change anymore, a steady state could be expected to have converged. They can be used [to](#) visualize the simulation results and to control if the flow regime seems unnatural or the mesh got disrupted during adaptations. Both happened in the process of finding suitable meshes.

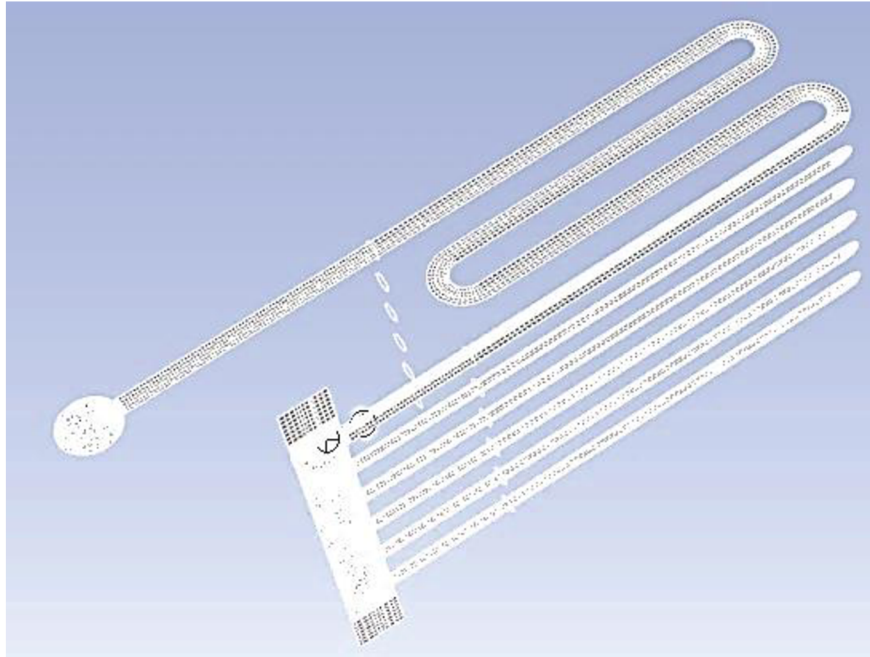


Figure 38: Control Surfaces (YZ-Plane trough the distributor, XZ-Plane trough the first serpentine and Monitors as well as Surfaces at the tube Inlets for reference pressures) and Points (one in the turbulent part of the distributor and one in the turbulent part of the first serpentine) for the evaluation of simulation results and convergence

The small $k-\omega$ mesh was only simulated in steady state. It converged in steady state and thus a transient case was not necessary to be calculated (Figure 39). The big $k-\omega$ mesh converged in steady state too but was still simulated in transient. Also, for the big $k-\omega$ mesh the residuals were set lower, as this solution is meant to be the most accurate and the one, the other simulations can be compared with. The calculation of the $k-\epsilon$ model did not converge in steady state but converged fast in transient and the solution was very stable over time.

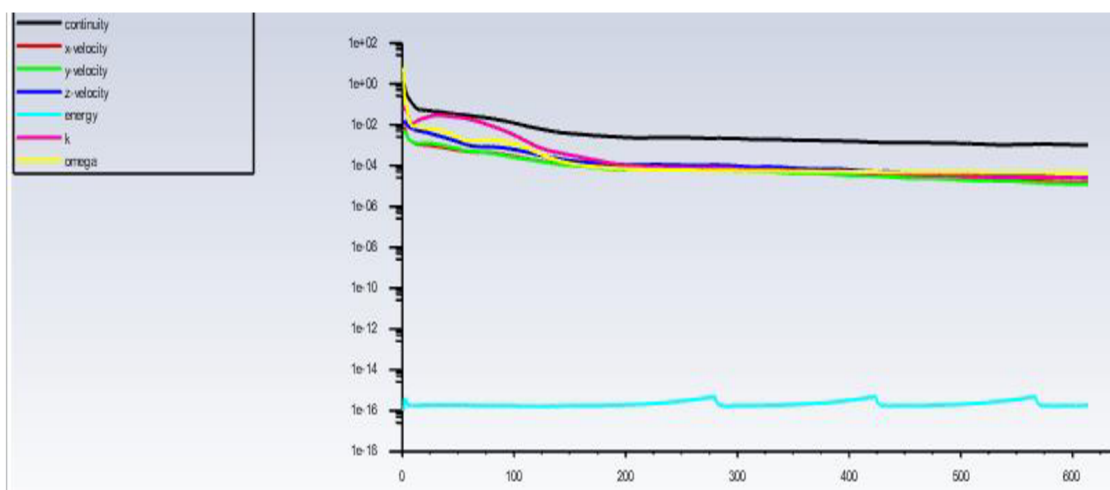


Figure 39: Residuals $k-\omega$ small – steady state

The big $k-\omega$ mesh as well as the $k-\epsilon$ case were first calculated in steady state until the residuals reached a plateau, then the calculation was continued in transient mode

(Figure 40). Different timesteps were tested to see they frequencies interfere with the stability of the solution or if the flow distribution oscillates. Then the size of the time steps was chosen, taking into account, that more than just a few seconds should be simulated to get a dependable average output and that the simulation for each time step should converge after a short time (i.e. not too many iterations per timestep needed). For the $k-\epsilon$ simulation the time steps were 0,20 seconds while the $k-\omega$ case was simulated with time steps of 0,005 seconds.

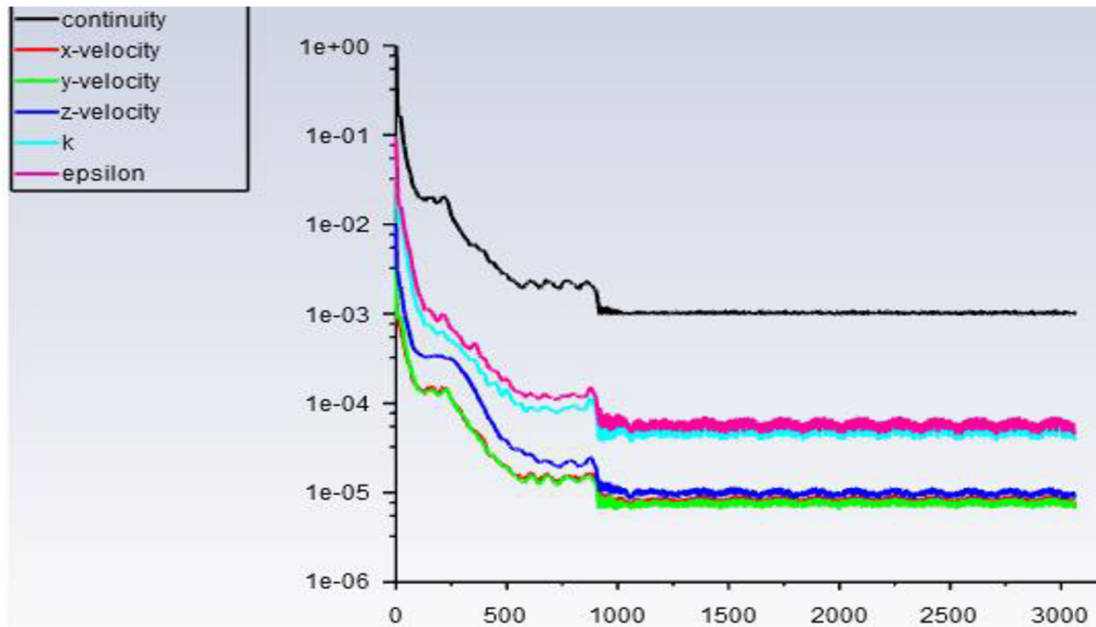


Figure 40: Residuals $k-\epsilon$ - steady state – transient 0,2s timesteps

3.3 Main results of CFD simulation

The overall results for flow distribution of all three simulations look quite similar. The highest deviation of the mass flow rate from the target is at the first serpentine pipe. Still there are differences, especially in the modulation of the viscous layer between the various simulations, which is the source of the main differences in the predicted flow. The higher the resolution of the mesh, the thinner the viscous layer seems to become, as flow regime near the wall is solved more accurately. Even the flow in the middle of the geometry seems to higher gradients in velocity with increasingly fine mesh. This might also be connected to the size of the cells. The simulation with the big $k-\omega$ mesh seems to be the most distinctive with a dense high velocity flow on the lower side of the entered serpentine pipe (Figure 42). A similar picture is given for the solution of the small $k-\omega$ mesh. The main difference here seems to be, that the transition from fast to slow velocities in the stream are smoother. The viscous layer seems thicker, too (Figure 41). The smoothest transitions in the flow are to be see in the solution for the $k-\epsilon$ model. The distribution of the flow velocity and the viscous layer seem more even and is thicker than in the high resolution $k-\omega$ solution (Figure 43). The more even viscous layer, for $k-\epsilon$ in comparison to $k-\omega$, was expected as it is calculated with the Non-Equilibrium Wall Function and not by solving the nearfield of the wall. The smoothness of the transition should not be taken as an indicator of quality of the solution in this case. It is simply the result of the wall function, which is ranked below a solution solving the viscous layer with enough calculation points, in terms of accuracy.

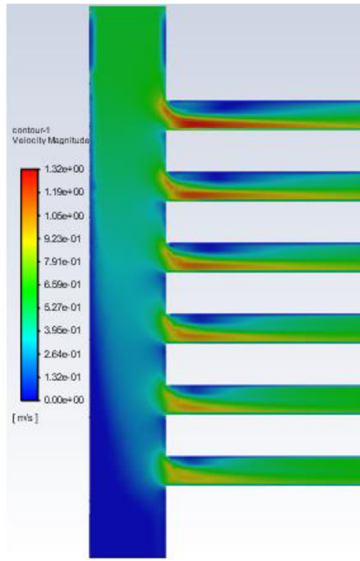


Figure 41: contour plot of velocity in YZ-plane of the distributor and serpentine (k- ω small); (scale [0; 1,32] m/s)

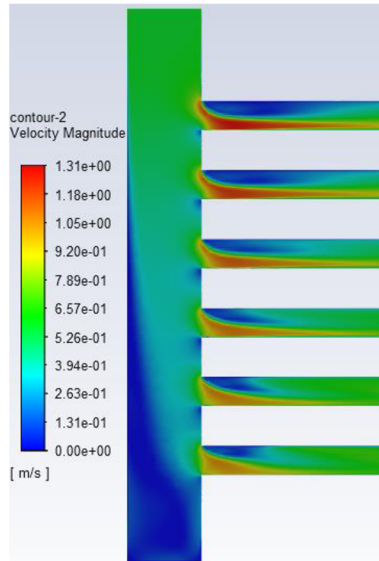


Figure 42: contour plot of velocity in YZ-plane of the distributor and serpentine (k- ω big); (scale [0; 1,31] m/s)

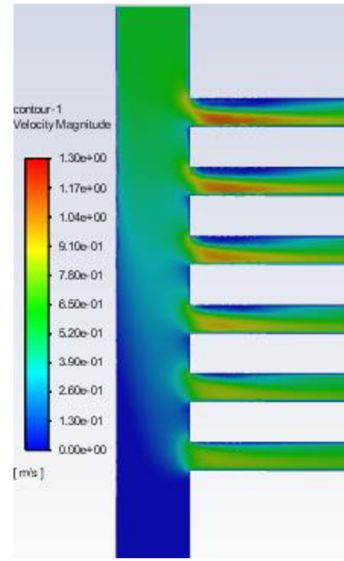


Figure 43: contour plot of velocity in YZ-plane of the distributor and serpentine (k- ϵ); (scale [0; 1,3] m/s)

Figure 44 shows a vector plot of the high-resolution k- ω results in the YZ-plane. The shown part consists of the first two pipes entered by the flow. As the vectors show, there is a slow backflow on the upper part of the pipes, where the flow enters. This phenomenon is stronger in the upper tubes.

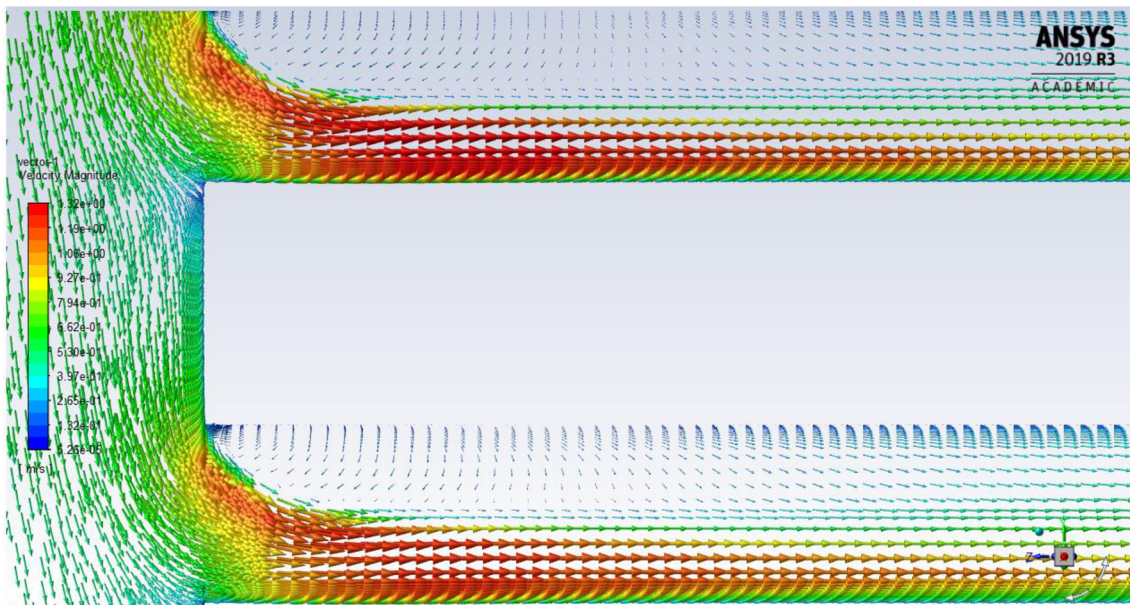


Figure 44: Vector plot of middle plane of the two upper Serpentine inlets (k- ω big) (scale [0; 1,32] m/s)

As mentioned, the transient simulation was only carried out for the big k- ω case and the k- ϵ case. The solution for the k- ω model seems quite unsteady, but the mass flow rates

for each tube seem to oscillate an average value in a chaotic manner (Figure 45). The simulation was carried out with at time stepping of 0,005 s. The blue straight line in the following three figures resembles the target mass flow rate for a perfectly even distributed flow.

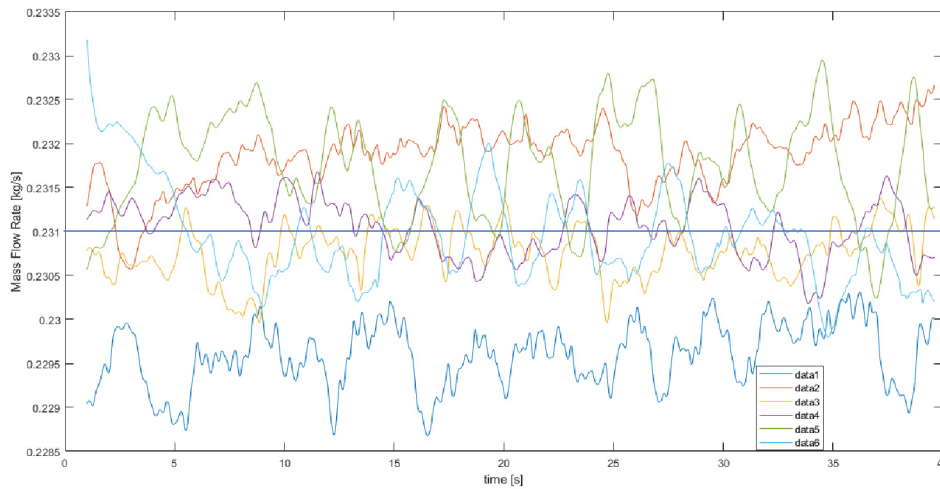


Figure 45: Plot of Mass Flow Rates over Time for big $k-\omega$ mesh - Time Steps of 0,005 s

In contrast to this the transient calculation for the $k-\epsilon$ case seems steady. The Beginning seems not to be steady, but it is to assume that this is due to the lack of a converged steady state solution at the start of the transient simulation. The mass flow rates barely alternate over time. The simulation could even be carried out with a 40 times bigger time stepping of 0,20 Seconds (Figure 46).

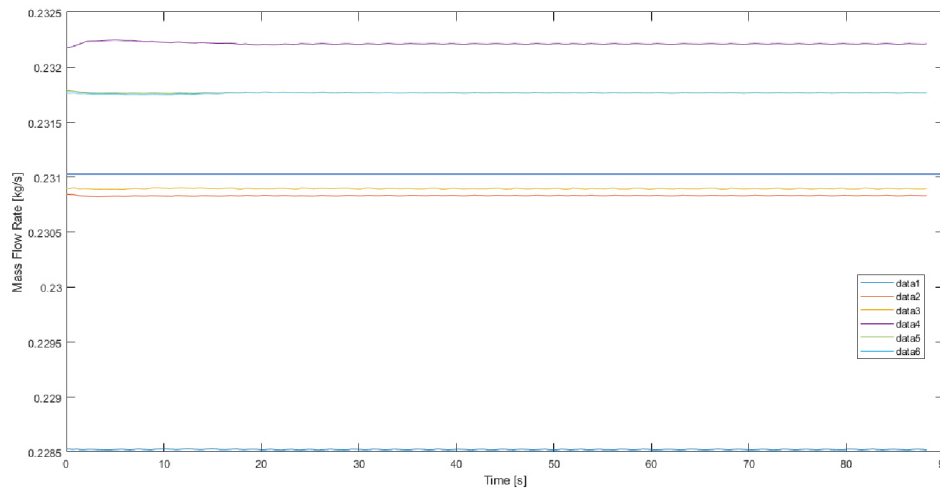


Figure 46: Plot of Mass Flow Rates over Time for $k-\epsilon$ mesh - Time Steps of 0,20 s

As Figure 47 shows the results for the mass flow rate from the small $k-\omega$ case and the $k-\epsilon$ case are quite similar. The high-resolution $k-\omega$ case differs the most in the tubes 1, 2 and 4. All simulations predict the lowest mass flow rate in the first tube, connected to the distributor. The mass flow rates for each tube and case and (in case of transient simulation) the standard deviations are listed in Table 15.

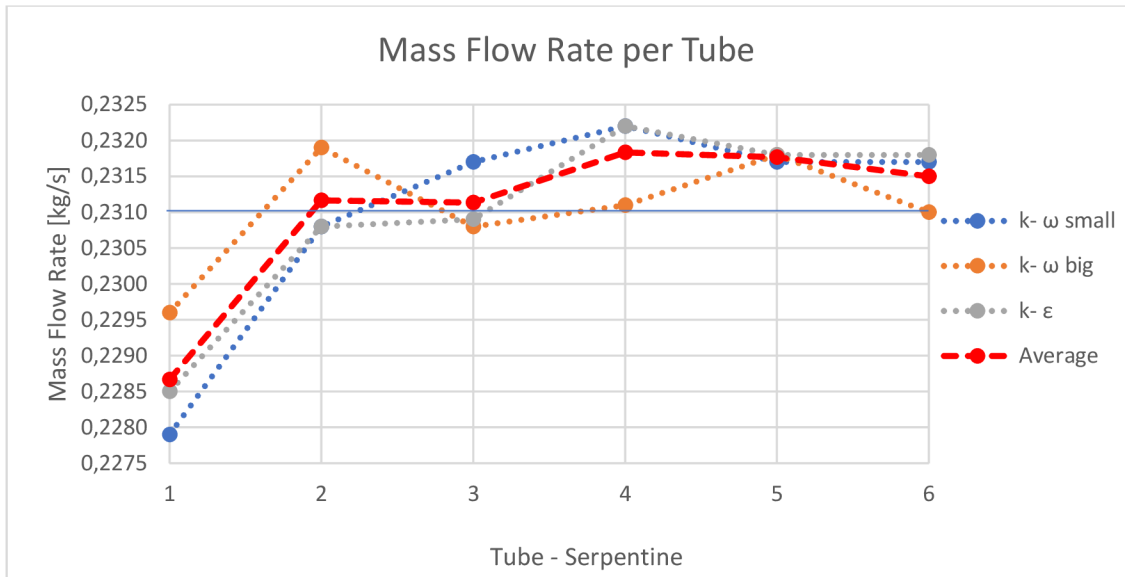


Figure 47: Mass flow distribution

Table 15: Mass Flow Rates and Standard Deviations for each case

	Target	Steady [kg/s]	Transient Mean [kg/s]			Standard Deviation	
	[kg/s]	k-ω small	k-ω big	k-ε	Average	k-ω big	k-ε
M1	0,231	0,2279	0,2296	0,2285	0,2287	$3,6058 \cdot 10^{-4}$	$3,0043 \cdot 10^{-6}$
M2	0,231	0,2308	0,2319	0,2308	0,2312	$3,6680 \cdot 10^{-4}$	$3,0836 \cdot 10^{-6}$
M3	0,231	0,2317	0,2308	0,2309	0,2311	$2,9137 \cdot 10^{-4}$	$2,6932 \cdot 10^{-6}$
M4	0,231	0,2322	0,2311	0,2322	0,2318	$3,2240 \cdot 10^{-4}$	$8,8550 \cdot 10^{-6}$
M5	0,231	0,2317	0,2318	0,2318	0,2318	$5,9092 \cdot 10^{-4}$	$3,3485 \cdot 10^{-6}$
M6	0,231	0,2317	0,2310	0,2318	0,2315	$5,5092 \cdot 10^{-4}$	$5,4365 \cdot 10^{-6}$
Sum	1,386	1,386	1,386	1,386	1,3861		

As to see in Table 16 the highest difference in the mass flow rate in a tube between any of the three simulations, and to the ideally distributed mass flow rate is -1,34%. According to the simulations the flow distribution is quite even.

Table 16: Deviation of Target Mass Flow Rates for each tube and for each case in percent

	k-ω small	k-ω big	k-ε
M1	-1,34%	-0,61%	-1,08%
M2	-0,09%	0,39%	-0,09%
M3	0,30%	-0,09%	-0,04%
M4	0,52%	0,04%	0,52%
M5	0,30%	0,35%	0,35%
M6	0,30%	0,00%	0,35%

The tube-side pressure drops, were evaluated in a similar manner as in case of HTRI simulations. The obtained results are listed in Table 17. The HTRI results were close to, or the same as the target of maximum 1 kPa. The simulation gives out results that are

well below that value. It is to mention that for the evaluation of the pressure drops in the simulation, the *Area Weighted Averages* of the faces in the tubes where the flow enters the inside of the shell, were selected. This neglects the highly turbulent flow in the tube mouths and thus is to be taken with caution. That is because the pressure drops in the collector, the distributor and the tube mouths sum up to more than one third of the total pressure drop of the whole heat exchanger module. As in addition to this the geometry in comparison to the geometry used for the HTRI simulation was changed, a direct comparison of values does not make much sense. Nonetheless both simulations state, that the pressure drops in the serpentines is within range.

The values in **Table 17** show a huge difference in total pressure drop between the high resolution (k- ω big) solution and the solutions with a less accurate prediction of the viscous layer (k- ω small; k- ϵ). This difference of up to 12 % in total pressure drop was not to foresee, just looking at the flow distribution. It is a good example for how important the accuracy of solution for the viscous layer is for the simulation results. It might not have affected the solution for the flow distribution in a significant manner, but if for example heat transfer would have been simulated, huge differences would be expected.

Table 17: Inlet and outlet pressures in Tubes and Total Pressure drop of Heat Exchanger Module In- to Outlet

[Pa]	Tube inlet			Tube outlet			Difference		
	k- ω small	k- ω big	k- ϵ	k- ω small	k- ω big	k- ϵ	k- ω small	k- ω big	k- ϵ
1	976	1041	977	143	153	124	833	888	853
2	1033	1086	1019	178	177	148	855	908	872
3	1074	1129	1053	210	232	169	864	898	884
4	1105	1151	1084	233	247	194	872	903	890
5	1119	1153	1106	249	246	209	870	907	897
6	1120	1166	1107	244	261	206	876	905	901
Mean	1071	1121	1058	210	219	175	862	902	883
	Distributor Inlet			Collector Outlet					
Total	1383	1504	1322	0	0	0	1383	1504	1322

Figure 49 and Figure 48 show part of the development of the static pressure along the flow. As to expect, along the flow and in regions where local high velocities occur, drops in the static pressure are to be observed.

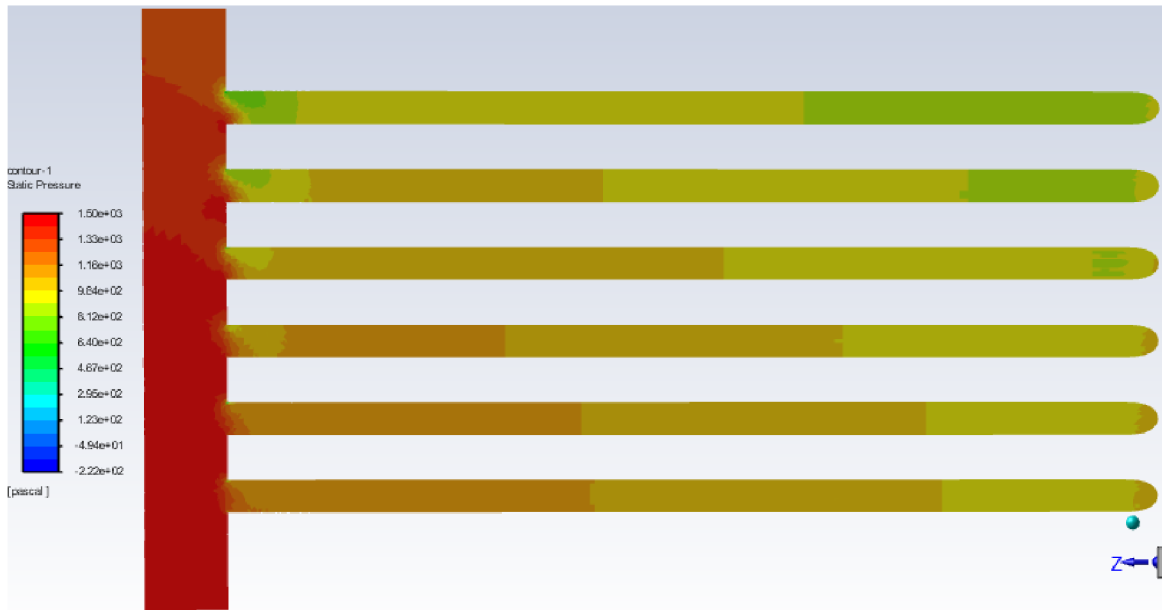


Figure 48: Contour Plot of Static pressure in the YZ-plane of the distributor with first straight parts of the tubes (k-ε simulation)

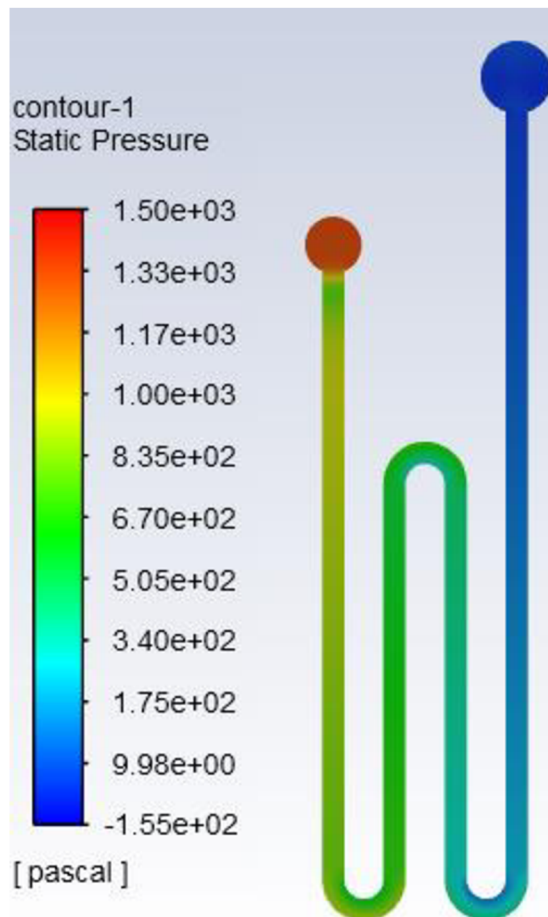


Figure 49: Contour Plot of Static Pressure in the XZ-Plane of the first serpentine (k-ε simulation)

4 Conclusion

The main objective of this thesis was to get acquainted with the design of a modular, tubular type heat exchanger with crossflow of fluids. To determine appropriate dimensions of the heat exchanger, the software HTRI employing thermal-hydraulic calculations was used. Furthermore, an evaluation of the flow distribution within one heat exchanger module was to carry out. For this a CFD simulation with Ansys Fluent was used.

The first chapter informs about the requirements for heat exchangers, used for waste heat utilization and the basic thermal and hydraulic equations for the dimensions' estimation of a heat exchanger are given.

The second chapter briefly explains the current layout situation at the burner testing laboratory at UPI. Furthermore, the use of the software HTRI in simulation mode for estimating the performance of the proposed heat exchanger is described. The results are compared with the target performance and the design is found to be sufficient.

The evaluation of the water flow distribution inside the heat exchanger tube bank module based on the result of CFD simulations is discussed in chapter three. Here three different CFD simulation approaches were made and compared. The creation of the model, including meshing and the setting of boundary conditions is described for each approach. Despite of quite big differences in the approaches all three methods have proven to be adequate for predicting the flow distribution of the simulated heat exchanger module. The result of the simulation is that the flow distribution is quite even. Still differences in the results are obvious as for example the calculated total pressure drop of the high-resolution k- ω model is about 12% higher than the one according to the calculation of the k- ϵ model.

In summary the results of the CFD and the HTRI simulations show, that the flow parameters on tube side are within range of the requirements and thus the design is sufficient in these regards. With the Initial design, that was used to perform the HTRI simulation the targeted heat duty was reachable. As the design changed due to manufacturing requirements, this result is now questionable, as the straight part of the serpentine was reduced from 400 mm to 375 mm. This reduces the modular tube length for heat exchange by $6 \times 25 \text{ mm} = 150 \text{ mm}$, and the total tube length by $4 \times 6 \times 25 \text{ mm} = 600 \text{ mm}$. This equals a decrease in heat exchange area of about 2,6 %. Furthermore, the wall thickness of the tubes was increased. Both these features result in a smaller achievable heat duty. Nevertheless, the design should still be sufficient, in the case of relatively clean tubes. Considering fouling of tubes, as the temperature of the cooling fluid is not rising that significantly in comparison to the hot fluid temperature, it is questionable whether the probably occurring shortcomings in heat exchange could be compromised by a higher flow rate of the cooling fluid.

The CFD simulation of the flow was far more challenging than expected. This was due to the meshing process, that produced bad quality cells right in the most critical areas of the flow. Therefore a long process of trial and error was necessary to obtain meshes of acceptable quality. This shows, that for efficient work with the meshing tool, experience is the key. Due to this time-consuming procedure a simulation of heat transfer was not possible anymore. A simulation of heat transfer would only have been possible with the big k- ω mesh. As this mesh is quite large, a simulation like that would have taken a long time. Since the flow data and the mesh are now already available, the simulation of heat transfer should not be too challenging, but very time-consuming and computationally expensive.

The work behind this thesis was an interesting process of gaining knowledge and experience, especially in the field of CFD simulation. One of the main lessons learned is to never underestimate the effort needed to obtain a suitable mesh, even for seemingly uncomplicated geometries.

For future work, the HTRI simulation could be redone with the actual design, and the heat exchange could be simulated and compared with collected data from the heat exchanger in operation.

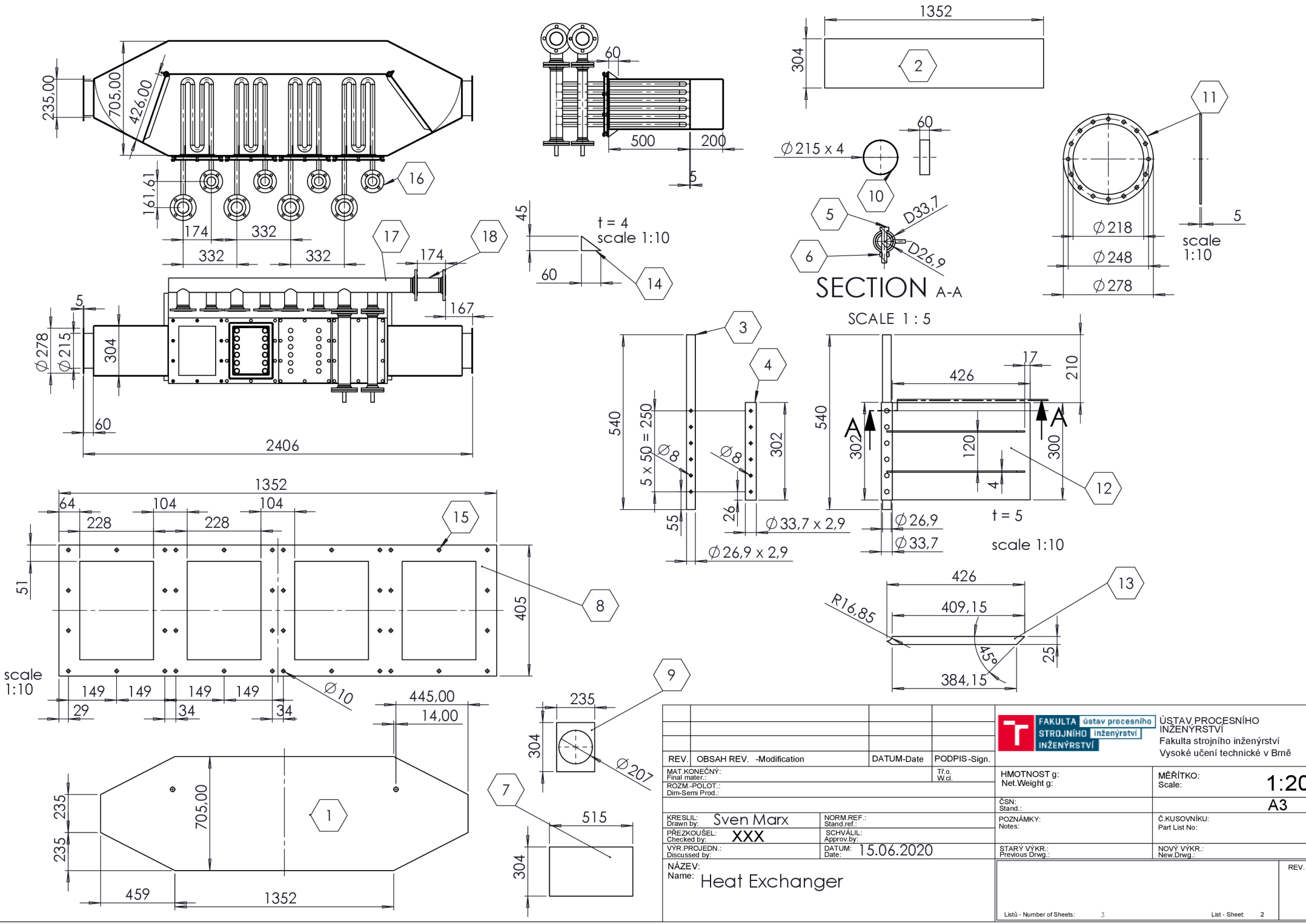
References


- [1] *Handbook of Thermal Science and Engineering*. Cham: Springer International Publishing, 2018.
- [2] T. Han, C.'a. Wang, Q. Cao, W. Chen, and D. Che, "Investigation on Heat Transfer Characteristics of the H-type Finned Tube in Flue Gas with High Content of Ash," *Energy Procedia*, vol. 105, pp. 4680–4684, 2017, doi: 10.1016/j.egypro.2017.03.1014.
- [3] *Heat exchanger fouling cleaning system*. [Online]. Available: <https://www.geurtsheatexchangers.com/products/heat-exchangers/heat-exchanger-fouling-cleaning-system/> (accessed: Dec. 30 2019).
- [4] *Flue Gas Heat Exchanger*. [Online]. Available: <http://www.shineheat.com/Flue-Gas-Heat-Exchanger.html> (accessed: Dec. 30 2019).
- [5] *VDI Heat Atlas*. Berlin, Heidelberg: Springer Berlin Heidelberg, 2010.
- [6] S. M. Salim, "International MultiConference of Engineers and Computer Scientists, IMECS 2009: 18 - 20 March, 2009, Regal Kowloon Hotel, Kowloon, Hong Kong," 2009.
- [7] J. F. Gülich, *Centrifugal Pumps*. Cham: Springer International Publishing, 2020.
- [8] Ansys Theory Guide, 4.3.3. *Realizable k- ϵ Model*. [Online]. Available: https://ansyshelp.ansys.com/account/secured?returnurl=/Views/Secured/corp/v191/flu_th/flu_th_sec_turb_realizke.html (accessed: May 19 2020).
- [9] Ansys Theory Guide, 4.16.4. *Non-Equilibrium Wall Functions*. [Online]. Available: https://ansyshelp.ansys.com/account/secured?returnurl=/Views/Secured/corp/v192/flu_th/flu_th_noneqwf.html?q=Non-Equilibrium%20Wall (accessed: May 19 2020).

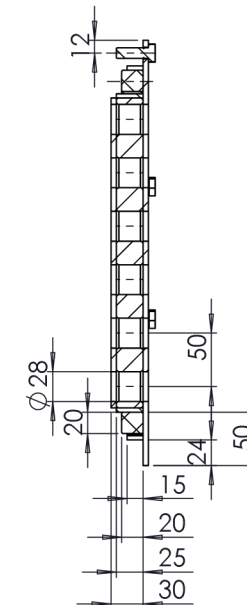
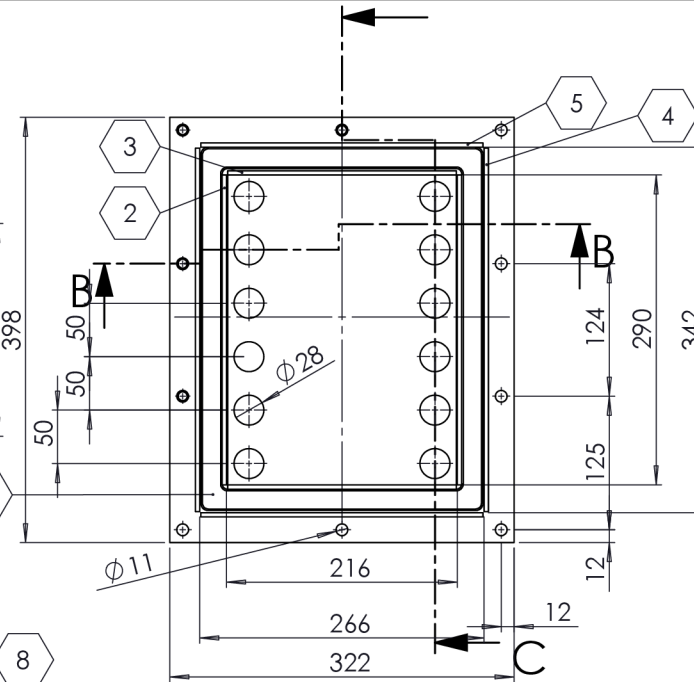
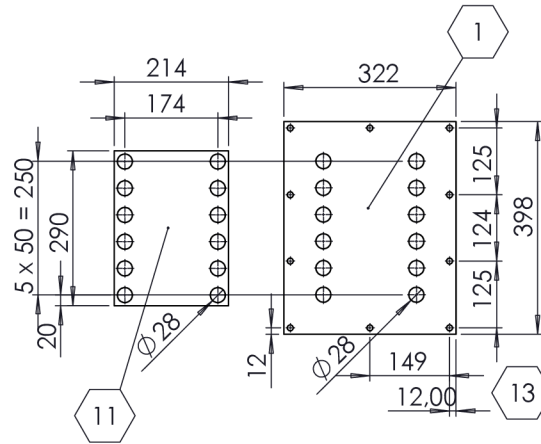
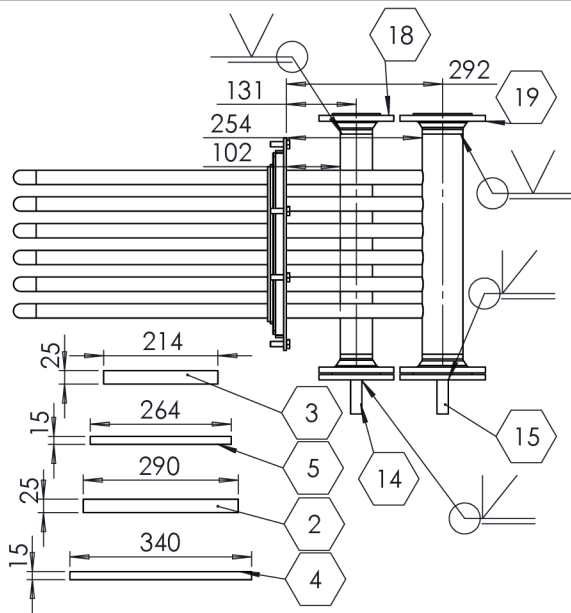
Appendix

Assembly drawings

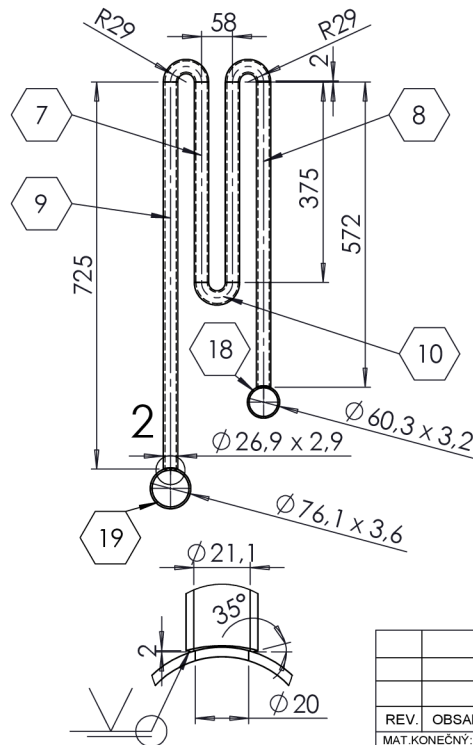
- Modular Heat Exchanger and Water Pipes
- Heat Exchanger
- Heat Exchanger Module



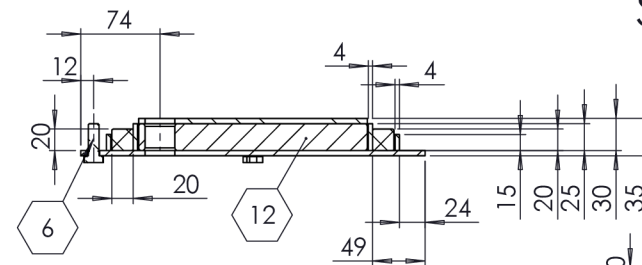
REV. OBSAH REV. -Modification DATUM -Date PODPIS -Sign.		 FAKULTA Ústav procesního STROJNÍHO inženýrství INŽENÝRSTVÍ	ÚSTAV PROCESNÍHO INŽENÝRSTVÍ Fakulta strojního inženýrství Vysoké učení technické v Brně	
MAT. KONEČNÝ: Final mater.: Tr.o. / W.cd.			HMOTNOST g: Net Weight g:	MĚŘITKO: Scale: 1:20
KRESLIL: Sven Marx Drawn by:		ČSN: Stand.:	A3	
PREZKOŮSEL: XXX Checked by:		POZNÁMKY: Notes:	Č. KUSOVNIKU: Part List No.:	
VYR. PROJEDN.: Discussed by:		SCHVALIL: Approv. by:	NOVÝ VÝKR.: New Drwg.:	
DATUM: 15.06.2020 Date:		STARÝ VÝKR.: Previous Drwg.:	REV.	
NÁZEV: Name: Heat Exchanger		Listů - Number of Sheets: 3 List - Sheet: 2		



Item Nr.	Part	Quantity
1	Sheet 398x322x5	1
2	Sheet 290x25x4	2
3	Sheet 214x25x4	2
4	Sheet 340x15x4	2
5	Sheet 264x15x4	2
6	Screw_M10	10
7	D25 x 375	12
8	DN25 x 572	6
9	DN25 x 725	6
10	DN25 Bend 180°	18
11	Sheet 290x214x5	1
12	insulation	1
13	Sealing 20x 20	1
14	Dead End Flange DN50-DN20	1
15	Dead End Flange DN65-DN20	1
16	Pipe_DN50x 3,2 L=412 (Distributor)	1
17	Pipe_DN65x3,6 L=412 (Collector)	1
18	Flange_DN50 PN6	2
19	Flange_DN65 PN6	2

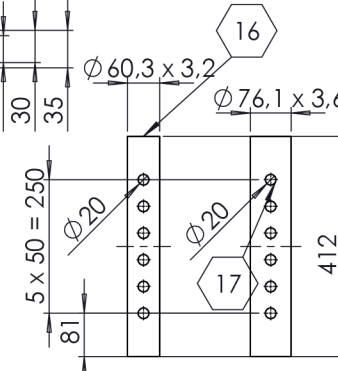


DETAIL 2
SCALE 1 : 2



SECTION B-B
SCALE 1 : 5

SECTION C-C
SCALE 1 : 5



REV. OBSAH REV. -Modification DATUM -Date PODPIS -Sign.		FAKULTA Ústav procesního strojnictví ÚSTAV PROCESNÍHO INŽENÝRSTVÍ Fakulta strojního inženýrství Vysoké učení technické v Brně	HMOTNOST g: Net Weight g:	MĚŘITKO: Scale:	1:10
MAT. KONEČNÝ: Final mater.:	Tř.o. W.cd.		ČSN: Stand.:	Č. KUSOVNIKU: Part List No:	A3
KRESLIL: Drawn by:	PREZKOŮSEL: Checked by:	NORM. REF.: Stand. ref.:	POZNÁMKY: Notes:	NOVÝ VÝKR.: New Drwg.:	REV.
VYR. PROJEDN.: Discussed by:	DATUM: Date:	SCHVÁLIL: Approv. by:	STARÝ VÝKR.: Previous Drwg.:		
NÁZEV: Name:		Heat Exchange Module			
Listů - Number of Sheets:		3		List - Sheet:	
				3	